AD-A062 093 BRISTOL UNIV (ENGLAND) DEPT OF AERONAUTICAL ENGINEERING F/G 20/4
PRESSURES ON A SLENDER, AXISYMMETRIC BODY AT HIGH ANGLE OF ATTA--ETC(U)
SEP 78 B L HUNT, P C DEXTER DA-ERO-77-G-073
UNCLASSIFIED BLH/7801 NL

1 OF 1
AD A062093

END
DATE FILMED
3-79
DDC

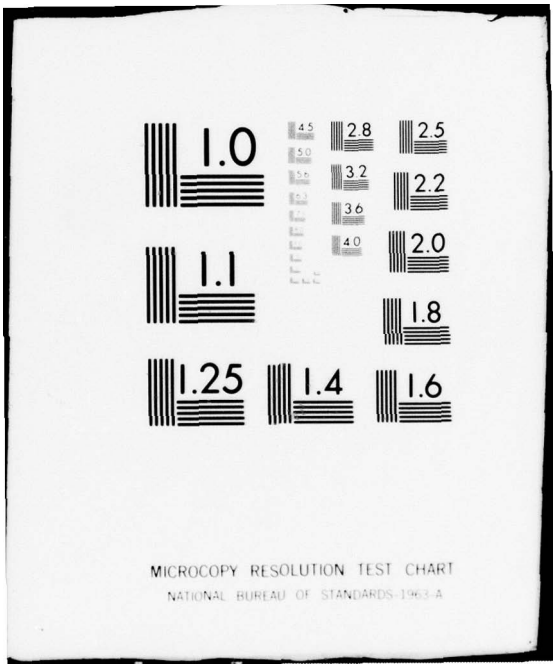
1.0
1.1
1.25
1.4
1.6
1.8
2.0
2.2
2.5
2.8
3.2
3.6
4.0
4.5
5.0
MICROCOPY RESOLUTION TEST CHART
NATIONAL BUREAU OF STANDARDS-1963-A

LEVEL II

AD

Report No. BLH/7801

UNIVERSITY OF BRISTOL

DEPARTMENT OF
AERONAUTICAL ENGINEERING

PRESSURES ON A SLENDER, AXISYMMETRIC BODY AT HIGH ANGLE OF ATTACK IN A VERY LOW TURBULENCE LEVEL AIR STREAM.

First Annual Report, no. 1 Aug 77-Aug 78,

by

B. L. Hunt and P. C. Dexter

September 1978

58 p.

U.S. ARMY EUROPEAN RESEARCH OFFICE
AND
U.S. AIR FORCE EUROPEAN OFFICE OF AEROSPACE RESEARCH AND DEVELOPMENT
London • England

1T161102BH57

AF

GRANT NUMBER DA-ERO-77-G-073

409 571

R&D 2450

REPORT DOCUMENTATION PAGE		READ INSTRUCTIONS BEFORE COMPLETING FORM
1. REPORT NUMBER	2. GOVT ACCESSION NO.	3. RECIPIENT'S CATALOG NUMBER
4. TITLE *(and Subtitle)* Pressures on a Slender Axisymmetric Body at High Angle of Attack in a very Low Turbulence Level Air Stream		5. TYPE OF REPORT & PERIOD COVERED Annual Technical Report August 77 - August 78 6. PERFORMING ORG. REPORT NUMBER
7. AUTHOR(s) B. L. Hunt P.C. Dexter		8. CONTRACT OR GRANT NUMBER(s) DAERO-77-G-073
9. PERFORMING ORGANIZATION NAME AND ADDRESS University of Bristol U.K.		10. PROGRAM ELEMENT, PROJECT, TASK AREA & WORK UNIT NUMBERS 6-11-02A-IT161102BH57-06-00-673
11. CONTROLLING OFFICE NAME AND ADDRESS U.S. Army R&S Group (Eur) Box 65 FPO NY 09510		12. REPORT DATE 13. NUMBER OF PAGES 56
14. MONITORING AGENCY NAME & ADDRESS*(if different from Controlling Office)*		15. SECURITY CLASS. *(of this report)* Unclassified 15a. DECLASSIFICATION/DOWNGRADING SCHEDULE

16. DISTRIBUTION STATEMENT *(of this Report)*

Release of Claims
Distribution unlimited

17. DISTRIBUTION STATEMENT *(of the abstract entered in Block 20, if different from Report)*

18. SUPPLEMENTARY NOTES

19. KEY WORDS *(Continue on reverse side if necessary and identify by block number)*

High angle of attack. Bodies of revolution. Side forces. Low speed. Low turbulence. Vortex flow fields. Laminar flow.

20. ABSTRACT *(Continue on reverse side if necessary and identify by block number)*

The report describes experimentally measured transient pressures at low speeds on a model consisting of a circular cylinder with four different interchangeable tangent ogive noses in the angle of attack range from 30° to 90°. Great care was taken to eliminate extraneous disturbances: a wind tunnel with an extremely low level of free stream turbulence (approx. 0.01%) was used, the model was rigidly mounted and efforts were made to ensure laminar separation without turbulent re-attachment. By comparing

20. the results with those obtained previously on the same model in similar tests at a higher level of free stream turbulence (approx. 0.7%) it is shown that there is a dramatic reduction in unsteadiness in the low turbulence level air stream and switching of the flow pattern is virtually eliminated. However, it is also found that the mean unswithced level is dependent on the roll angle of the model and hence that strict control of the free stream conditions is not sufficient to guarantee results which are independent of the experimental equipment. Details of the inherent unsteadiness present in the flow pattern are presented.

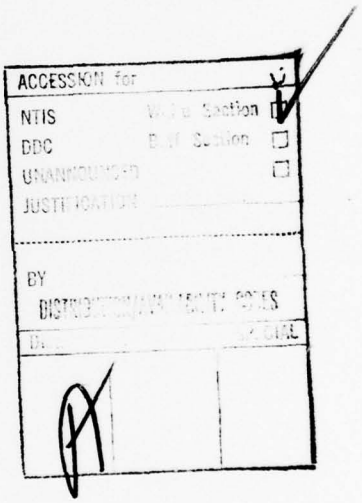

SUMMARY

This report describes experimentally measured transient pressures at low speeds on a model consisting of a circular cylinder with four different interchangeable tangent ogive noses in the angle of attack range from 30° to 90°. Great care was taken to eliminate extraneous disturbances: a wind tunnel with an extremely low level of free stream turbulence (approx. 0.01%) was used, the model was rigidly mounted and efforts were made to ensure laminar separation without turbulent re-attachment. By comparing the results with those obtained previously on the same model in similar tests at a higher level of free stream turbulence (approx. 0.7%) it is shown that there is a dramatic reduction in unsteadiness in the low turbulence level air stream and switching of the flow pattern is virtually eliminated. However, it is also found that the mean unswitched level is dependent on the roll angle of the model and hence that strict control of the free stream conditions is not sufficient to guarantee results which are independent of the experimental equipment. Details of the inherent unsteadiness present in the flow pattern are presented.

TABLE OF CONTENTS

INTRODUCTION

The existence of aerodynamic side forces on slender bodies of revolution at high angles of attack was first reported twenty-five years ago[1,2] but little further work was done during the subsequent fifteen years. Since the late 1960's, however, the desire to enlarge the flight envelopes of both missiles and military aircraft has promoted a large number of investigations of the phenomenon. References to many of these may be found in a paper by Nielsen[3], very recent work has mostly been reported in two AIAA conferences[4,5].

Despite the intensive research effort of the last ten years, very little understanding of the mechanisms by which the side force is determined has been achieved. One feature which has been established in numerous studies is that the side force is associated with an asymmetric vortex pattern in the lea of the body; an idealised sketch of the vortices is shown in Fig. 1. However, few reliable details of the vortex pattern are known and its relationship to the sectional side force distribution is not understood.

Probably the major barrier to progress has been the difficulty of obtaining meaningful experimental results. If the published data are studied, certain trends emerge but it is usually not difficult to find unexplained exceptions. Furthermore, large discrepancies exist between the results obtained by different workers and the data often do not vary smoothly with the independent parameters. The extent of the difficulty is illustrated by the study conducted by Wardlaw and Morrison[6]. They attempted to correlate all the measured values of overall side force against conventional flow and geometric parameters. However, they found the scatter to be so great that they were forced to adopt the view that these flows are non-deterministic and hence that the data must be treated by linear regression techniques.

Previous experimental studies have given some clues to the origins of these difficulties. One of the most striking peculiarities observed by most (but not quite all) of the experimenters who have looked for it is the variation (in both direction and magnitude) of the side force with roll angle. Work by Keener et al.[7,8] has provided strong evidence that this effect is somehow related to the detailed geometry or surface roughness of the tip of the nose. It is also a common experience that the force can be substantially altered by a change in surface conditions, such as is produced by a coat of paint. Again, the work of Keener et al.[8] provides evidence of this behaviour. It thus seems that one of the sources of experimental problems is an extreme sensitivity to details of the model, particularly to the condition of the nose.

Another cause of experimental difficulties is unsteadiness. Lamont and Hunt[9] recorded the transient behaviour of the difference between two surface pressure tappings at equal angles from the leading generator of the body. Two examples of the traces obtained are shown in Fig. 2. It is clear that in Fig. 2(a) a complete switch of the flow pattern has occurred from one state to its mirror image state. The trace in Fig. 2(b) is less

clear but again temporary changes in sign are present. After studying a large number of traces, Lamont and Hunt came to the conclusion that the major fluctuations are caused by a switching of the flow pattern towards and sometimes into the mirror image state. Since there appears to be a degree of stability in at least one of the two states, the switching must be caused by external disturbances. Lamont and Hunt suggested that the disturbances in their tests came from free stream turbulence. They showed by simple estimates that the observed behaviour was consistent with the scale and intensity of turbulence in the wind tunnel. They have pointed out[10,11] that model vibration is another source of external disturbances which is likely to cause switching. It is clear that if Lamont and Hunt are correct, then time averaged measurements which are taken in the presence of unsteadiness will depend on the free stream turbulence level and on the dynamic behaviour of the model support. Clark[12] has observed the wake flow using a water tunnel and he supports the notion that unsteadiness is due to free stream turbulence and to model vibration. However, he suggests that the transient behaviour is more complex than that proposed by Lamont and Hunt. According to Clark, a number of different vortex patterns can exist and the flow jumps from one pattern to another under the influence of external disturbances.

Lamont and Hunt's transient records showed differences in switching pattern with roll angle while the inferred unswitched levels seemed to be unaffected. This lead Lamont and Hunt to suggest[10,11] that the observed influence of roll angle on the time averaged readings would be eliminated if the unsteadiness were eliminated. Some support for this possibility is given by the fact that results which are independent of roll angle have, occasionally, been obtained[13,14].

The work reported here sets out to check Lamont and Hunt's notion of the importance of free stream turbulence. Great care has been taken to avoid switching. Lamont and Hunt's simple estimate[9] of the effect of free stream turbulence indicates that switching should virtually cease when the turbulence level is reduced to 0.1%. However, this value is unlikely to be very accurate and a wind tunnel has been chosen with the lowest turbulence level that is likely to be achievable in practice, approximately 0.01%. The other features of the experiment are that the model is extremely rigidly clamped and an attempt has been made to avoid turbulent reattachment of the flow. The model used is the same as that used by Lamont and Hunt and hence a comparison of the present results with those obtained earlier by Lamont and Hunt shows the direct effect of a change to a wind tunnel of much lower free stream turbulence.

Part of this work is to be reported at the AGARD Symposium on High Angle of Attack Aerodynamics[18] and, where appropriate, sections of the text of Reference 18 have been incorporated in this report.

2. APPARATUS

Results will be presented from both the Bristol University 2.1 m x 1.5 m wind tunnel and the Royal Aircraft Establishment 1.2 m x 0.9 m wind tunnel. Both are low speed tunnels. The R.A.E. tunnel has a contraction ratio of 31:1 which gives a streamwise turbulence level of approximately 0.01% over roughly the central 1 m x 0.8 m of the tunnels. Full details of the tunnel characteristics are given in References 15-17. No direct measurements of turbulence level have been carried out as part of the current series of tests but the level of pressure fluctuations on the model at zero incidence has been obtained and will be discussed later. The Bristol tunnel has a much smaller contraction ratio (5:1). This and other factors contribute to producing a streamwise turbulence level of approximately 0.7%[19]. This is quite high for a low speed tunnel but low compared to the level which might be expected in transonic or supersonic facilities, where many overall force measurements have been made.

The same model was used in both tunnels. It is the transient model of Lamont and Hunt's tests[9], a sketch can be seen in Fig. 3. The constant diameter section is 51 mm in diameter and contains four pressure tapped stations spaced 51 mm apart, each with four pairs of pressure tappings, as shown in Fig. 3. The nose of the model can either be fitted directly on to the measuring section or on to an untapped section of length four diameters which is then attached to the measuring section; it is thus possible to obtain measurements at one diameter spacing extending from one diameter to eight diameters from the nose junction. Four sharp tangent ogive noses were used, the length to maximum diameter ratios being 1, 2, 2.5 and 3: most of the results were obtained with the second and fourth of these noses. A constant diameter rear support section completes the model: this was clamped rigidly to the floor and roof of the tunnel by means of a 51 mm diameter vertical pylon. The clamps were located some six diameters aft of the most rearward measuring station. Any angle of attack in the range 0 to 90^{o} could be achieved. No vibration of the nose tip was visible when running except a slight motion at angles of attack around 70^{o}. In the R.A.E. tunnel, the nose could be observed through a telescope which would have revealed a movement of ± 0.02 mm.

The surface pressures were recorded as the difference between two points symmetrically disposed about the plane of incidence, such a difference being clearly related to the side force. The vast majority of results were obtained using the pair of tappings located at ± 75^{o} from the leading generator but some measurements were made from the other pressure holes in order to check that the behaviour was consistent around the circumference. The arrangement of holes illustrated in Fig. 3 allows 6 roll positions in which a pair of holes are at ± 75^{o}, thus enabling some investigations of sensitivity to roll angle. In the Bristol tunnel and in early tests in the R.A.E. tunnel, the pressure difference was obtained by connecting the pressure tappings across a ± 0.1 p.s.i.d. Scanco variable

reluctance transducer mounted inside the model. However, some concern was felt at feeding a fluctuating pressure to the back of the transducer and a new system was adopted. This used two transducers, each connected to one of the ports and with a common steady backing pressure (the tunnel free stream static pressure, appropriately damped); the difference of the outputs was then taken electrically. In this arrangement, the two transducers were Setra ± 0.1 p.s.i.d. variable capacitance type. Figure 4 shows traces from identical tests in the R.A.E. tunnel using the two different systems. It can be seen that there is no significant difference between them. The results obtained with a single transducer are therefore believed to be entirely reliable. Nonetheless, the second arrangement is preferable in principle and was retained. In all cases, the pressure tubing was kept as short as possible. The system was estimated to be able to respond to a signal of 400 Hz without significant attenuation[20]. The output was passed via a drive amplifier to an ultra-violet recorder.

3. TESTS CONDUCTED

Tests were conducted at values of Reynolds number in the range 0.4×10^5 to 2×10^5 where the Reynolds number is defined as $U\, d\, \mathrm{cosec}\alpha/\nu$ and U is the free stream velocity, d is the diameter of the cylindrical section, ν is the kinematic viscosity and α is the angle of attack. A justification for the use of this definition is given by Lamont and Hunt[9]. However, the question of most appropriate definition is by no means settled and alternative views may be found in References 12, 21 and 22. In any event, it was hoped that sufficient margin was left so that the results would not be influenced by turbulent reattachment (but see the discussion in Section 4.2).

The other major parameters which were varied were angle of attack, α, axial location of the measuring station, x/d, roll angle, ϕ, and nose fineness ratio, L_N/d. A total of about 400 tests were carried out. In addition, a few ad hoc tests were conducted to examine the effect of adding imperfections to the nose in the form of plastic tape of thickness 0.15 mm. The dimensions and locations of the tape are shown on Fig. 5.

In the next section, it will be seen that a careful check on the effect of roll angle was conducted. In these tests, it was necessary to be particularly sure that the pressure tappings were accurately symmetrical in all cases, the method adopted was as follows.

The model was set at 90° incidence and the roll angle was set to approximately 0°. A fine mark at the leeward side of the model exactly at the most rearward body generator ($\pm 180^\circ$) had been previously scribed on the model. The model was rolled until this mark was equidistant from the top and bottom sides of the model when viewed horizontally through a travelling microscope. With the model remaining at 90° incidence the mean value of the pressure difference was checked to ensure it was zero. A

square block was then clamped on to the end of the model downstream of the support clamp, and this was used, together with an accurate clinometer to re-set the model to any required roll angle. When each new roll angle was set up readings were taken at an incidence of 90° to check that the mean pressure difference was zero, before any measurements were made at other incidences.

4. PRESENTATION AND DISCUSSION OF RESULTS

The pressures were recorded on the ultraviolet recorder for each visual examination and most of the results presented here were traced directly from these records. Although this method is convenient for examining the qualitative behaviour, it is not so satisfactory when a quantitative analysis is required. In particular, there is bound to be a degree of subjectivity about the mean values and predominant frequencies which have been obtained, by hand, from the traces and this should be borne in mind when studying the results. It is intended that the transient behaviour will eventually be put on to an accurate, quantitative basis by feeding the pressure signals to a frequency analyser.

4.1 Zero angle of attack

Figure 6 shows traces obtained simultaneously from two ports in the same station on the model in the R.A.E. tunnel. Also shown is the difference in pressures. It can be seen that the disturbances present on the individual tappings are in phase and that the pressure difference is barely detectable. This situation is consistent with the disturbances being produced by plane sound waves. Now, the magnitudes of pressure, p', and velocity, u', fluctuations produced by plane sound waves are related by the expression

$$u' = \frac{p'}{\rho a} \qquad (1)$$

where a is the speed of sound. Taking the maximum amplitudes of the traces for the individual ports from Fig. 6, using eqn. (1) and assuming a simple sine wave form for the fluctuations, one obtains an estimate of 0.01% for the r.m.s. streamwise component of the turbulence. This is slightly higher than earlier measurements of the sound-induced turbulence level in this tunnel[16] (which were approximately 0.005% at the tunnel speed of Fig. 6) but considering the approximations necessary to obtain the current estimate, the two sets of values are acceptably close. These measurements provide a measure of the pressure fluctuations in the clean tunnel against which the values obtained at angle of attack can be compared. The amplitudes of the pressure coefficients, based on free stream dynamic head are $C_p' \simeq 0.013$ for the individual pressures and $C_p' \simeq 0.003$ for the pressure difference.

4.2 The three calibre nose

The results obtained with the three calibre nose ($L_N/d = 3$) can for

the most part be given a self-consistent interpretation. The results from the other noses are consistent with those from the three calibre nose but they do raise certain additional problems. We therefore consider the more straightforward case of the three calibre nose first.

4.2.1 Unsteadiness at angle of attack

One of the most important objectives of this work was to study the effect of conducting tests in the low turbulence flow on the fluctuating component of the surface pressures. It was found that, except for values of α near to 90°, the pressures in the R.A.E. tunnel were dramatically more steady than those in the Bristol tunnel. A good example is provided by Fig. 7 which is for a Reynolds number of 1.1×10^5 and $\alpha = 50^{\circ}$. The measuring station has been chosen close to the first peak of the sectional side force distribution, as determined from the time-averaged measurements of Lamont and Hunt[9]. The approximate location on this distribution is indicated on sketches on Fig. 7 and on subsequent figures. It should be noted that it cannot be taken as certain that the same distribution will apply in the R.A.E. tunnel.

It can be seen that the trace from the Bristol tunnel, Fig. 7(a), attains and holds roughly the level of Fig. 7(b) for brief intervals, but is subject to massive departures from this level and reverses sign from time to time. This behaviour is entirely consistent with the turbulence-induced switching suggested by Lamont and Hunt. Figure 7(b) shows that the non-switching flow does have a small inherent unsteadiness but that this is unbiased in direction and a meaningful time average of such a trace should be obtainable. Of course, the existence of reduced unsteadiness in the R.A.E. tunnel does not allow us to distinguish between the suggestion of a flow which switches between mirror image states and Clark's description of randomly occurring multiple states[12]. This question is therefore unresolved at present; on the one hand, there are the transient records, such as Fig. 7(a), which are more consistent with mirror image states and, on the other, there are Clark's observations and photographs[12].

As far as the frequency of the unsteadiness present in Fig. 7(b) is concerned, it is difficult to make any deductions from the trace except that the form bears little resemblance to classical Karman vortex shedding for which the frequency would be 77 Hz, based on the cross-flow velocity and a Strouhal number of 0.2.

When the angle of attack is reduced to 30°, the situation seen in Fig. 8 is produced. Again, the most important feature is the vastly reduced unsteadiness in the R.A.E. tunnel. On this occasion, however, the Bristol trace shows much greater instantaneous magnitudes than the R.A.E. record and it appears that the detailed action of the turbulent eddies is more complex than originally thought. The non-dimensional level of residual unsteadiness in the R.A.E. trace is approximately the same as that at $\alpha = 50^{\circ}$ (note the different scales on Figs. 7(b) and 8(b)) and is, of course, very much higher than the amplitudes measured when $\alpha = 0^{\circ}$. The

mean pressure difference has, however, fallen considerably. Again, Fig. 8(b) does not have any obvious content at the cross-flow Strouhal frequency which is 32 Hz.

Traces obtained for similar types of tests but at angles of incidence of 35°, 40°, 45° and 55° are shown in Figs. 9 and 10. The corresponding tests in the Bristol tunnel are not shown in these figures, but it can be seen that the nature of the results is similar to those shown in Figs. 7(b) and 8(b). The mean level increases with increase in incidence, and the magnitude of the unsteadiness does not change significantly with incidence (note the differences in scales on the figures). Counting the significant peaks in the traces to determine the dominant frequencies showed no content at the cross-flow Strouhal frequency in any of the cases.

Figure 11 presents traces obtained at $\alpha = 60^{\circ}$. In this case, the measurements were taken close to the second peak of the sectional side force distribution because the first peak occurs on the nose at this angle. Once again, the influence of the higher level of turbulence is strikingly illustrated. The non-dimensional amplitude of fluctuation in the R.A.E. tunnel is slightly higher in this case than at the lower angles although this may be due to the measurements being on the second peak (see later comments). The nature of the fluctuations is now much more regular and the frequency obtained by counting what were considered significant peaks produced a value of 104 Hz, which is very close to the cross-flow Strouhal frequency of 99 Hz.

Further aft along the body, at the last measuring station which is located at $x/d = 11$, the behaviour is even more close to Karman vortex shedding. The trace is presented in Fig. 12 (note the slightly lower value of Reynolds number). In this case, the mean value is almost zero and the fluctuations are relatively regular with an estimated frequency of 88 Hz which is virtually identical with the cross-flow Strouhal frequency of 90 Hz. This is not surprising since, at large distances from the nose, the body must behave like an infinite yawed cylinder, which is known to exhibit Karman vortex shedding.

As the angle of incidence increases the region of Karman vortex shedding moves nearer to the nose, and at $\alpha = 65^{\circ}$ the trace shown in Fig. 13(a) is obtained at $x/d = 4$. The relatively regular nature of the fluctuations can again be seen, and the estimated frequency is again virtually identical with the Strouhal frequency. The mean level of the non-dimensional pressure difference is still quite large, but as the incidence is increased yet further the measured pressure difference becomes very unsteady exhibiting the sort of behaviour shown in Fig. 13(b), obtained at an incidence of 70°. In this case the trace is very disturbed combining a mixture of small amplitude fluctuations, similar to those that might be expected from a Strouhal-type disturbance, with large changes attributable to "switching" type behaviour, where the pressure difference changes sign. (It is noteworthy that at this incidence the model was most

liable to show signs of vibration, induced by the oscillating nature of the pressure difference.) This switching is probably induced by the Strouhal "shedding" which is present. Although the non-dimensional pressure difference does achieve large values either side of zero, its mean level has fallen to approximately zero.

At an incidence of 75^{o} the trace presented in Fig. 14 is obtained which shows that the region of Karman vortex shedding has moved forward to the measuring station at x/d=5 and the mean level has fallen to almost zero. The estimated frequency is just about identical to the Strouhal frequencies. Observations of this kind were made previously by Lamont and Hunt[9] but it was thought to be worthwhile to confirm them under low turbulence conditions. It seems quite likely that the unsteadiness in the flow pattern near the nose is either some form of incipient vortex shedding or is induced by the forward transmission of information along the body from the rear portions where Karman vortex shedding exists.

The traces in the figures previously discussed were for a Reynolds number (based on D cosecα) of 1.0×10^5. Tests at other Reynolds numbers were also conducted, but always remaining within the subcritical region so that the boundary layer remains laminar up to separation. Figures 15 and 16 show the effect of increasing the Reynolds number from 0.7×10^5 to 1.4×10^5 at a constant incidence of $\alpha = 30^{o}$. Allowing for change of vertical scale it can be seen that as the Reynolds number increases the non-dimensional fluctuating component of the signal remains approximately constant and the mean level varies only slightly. The most obvious feature is that the frequency becomes greater with increasing Reynolds number from 102 Hz to 130 Hz as the Reynolds number changes from 0.7×10^5 to 1.4×10^5. (Note that this does not correspond to a constant Strouhal number.)

The results at an incidence of 50^{o} are shown in Figs. 17 and 18, where again the trend is for a slight change in the mean level with little change in the level of unsteadiness. The frequency changes from an estimated 112 Hz at Reynolds number 0.5×10^5 to 164 Hz at Reynolds number 1.1×10^5. The same trends are evident in results even for an incidence of 70^{o}, as shown in Figs. 19 and 20, where the trace is very disturbed in each case. The mean level remains approximately zero and the frequency of the unsteady component, whose non-dimensional magnitude remains almost independent of Reynolds number, changes from 72 Hz at Reynolds number 0.5×10^5 to 120 Hz at Reynolds number 1.0×10^5.

The nature of the traces allows only approximate values of $\Delta\overline{C}_p$ and $\Delta C_p'$ particularly, to be determined, but these values have been estimated and plotted against α for a Reynolds number of 0.7×10^5 in Fig. 21 and similarly but at a Reynolds number of 1.0×10^5 in Fig. 22. It can be seen that the small effect of Reynolds number on pressure levels which was described above was true for all incidences, and that the amplitude of the unsteadiness is roughly constant in the range $30^{o} < \alpha < 50^{o}$ and then rises rapidly as Karman vortex shedding develops.

During the course of the tests some recordings of the pressure difference ΔC_p were also made using different pressure tapping locations, at $\theta = \pm 45^o, \pm 105^o$ and $\pm 135^o$, where θ is the angle around the body from the leading generator. Some sample traces are shown for an incidence of 55^o in Fig. 23. (Note that the corresponding trace for $\theta \pm 75^o$ is shown in Fig. 10(b)). Both the mean level and the unsteadiness in ΔC_p increase as the pressure tapping moves rearward round the body into the separated region, but there are no significant differences such as whole scale changes of mean level within a single record or large frequency changes between the recordings. Also the unsteadiness remains sensibly a constant percentage of the mean level for each. The readings obtained at $\theta = \pm 75^o$, which are those used in the majority of the testing, are therefore seen to be typical of the behaviour around the entire circumference.

4.2.2 Effect of roll angle

The results presented in the above section appear to throw a good deal of light on the problem of unsteadiness and hold out considerable promise that meaningful time-averaged readings can be taken if a wind tunnel of suitable quality is available. The other source of difficulty is that of sensitivity to minute details in the experimental model; this problem normally shows up as a dependence on roll angle. A series of tests at different roll angles was therefore undertaken. Great care was taken to ensure that the model was correctly lined up each time.

Figure 24 shows three traces at different roll angles for $\alpha = 50^o$. It can be seen that the nature of the traces is similar but the mean levels vary by up to a factor of seven. This and similar results at other angles of attack show that the commonly observed dependence of overall force on roll angle is not due to different patterns of switching, as had been suggested by Lamont and Hunt[11], but is due to a genuine difference in the mean sectional side force. The variation in levels of disturbance with roll angle which were observed by Lamont and Hunt is most probably due to the fact that changing the mean level of side force in a stream of given turbulence results in a changing frequency of switching[9].

Figure 25 shows the traces obtained at the reduced value of Reynolds number of 0.5×10^5; it can be seen that there has been a small change in the mean level at $\phi = 0^o$ but, in general, the traces are very similar to the corresponding traces in Fig. 24.

Figure 26 shows the variation of the mean level of ΔC_p with α for the two roll angles 0 and 180^o; unfortunately, measurements for $\phi = 150^o$ (which shows the strongest effect) were only taken at $\alpha = 30^o$ and $\alpha = 50^o$ and are not shown on this figure. The station is not always precisely at the peak of the side force distribution (indeed above 55^o the first peak occurs on the nose and the values plotted correspond to the second peak). However, the relative magnitudes for the two roll angles are significant. It can be seen that the 0^o roll angle gives consistently higher values than the 180^o

roll angle. This raises the hope that the difference may be due to identifiable asymmetries on the model. In view of the results obtained by Keener et al.[7], any such imperfections seem likely to be located near the tip of the nose. The nose of the model was therefore checked for eccentricity and surface roughness by means of "Talyrond" and "Talysurf" machines respectively. The error in roundness of the nose is plotted in Fig. 27 which shows that over most of its length the nose cross-section does not depart from a circle by more than 0.021 mm. Note that the maximum value shown was obtained with the measuring stylus resting on the edge of the base of the section which had a slight indentation due to a knock. The angular positions relative to $\theta = o^{o}$ of the maximum and minimum radii of the cross-section at the measured stations are also shown on the figure. Clearly the positions do not remain constant over the length of the nose, so there is no obvious ridge or flat running along the length of the nose which could be the source of the roll angle dependence. It is difficult to imagine a mechanism by which the measured eccentricity can produce the large observed effects, although the possibility cannot be ruled out all together.

The surface roughness of a tip region of axial length length 20 mm was found to be uniform and the roughness height to be less than 0.002 mm. Nearer the base, larger, isolated grooves were found, the maximum depth being 0.004 mm. There were also a very few identifiable small marks of depth approximately 0.01 mm caused probably by mishandling of the model. These were of the form of small dents measuring in the order of 0.4 mm to 1.0 mm across. The join between the nose and the constant diameter section gave rise to a rather large step whose height was 0.165 mm at its maximum.

For a two-dimensional laminar boundary layer, it is generally believed that there is a critical value of roughness height below which the roughness has no effect[23,24,25]; above the critical value, transition occurs. The critical height, k_{crit}, for a single two-dimensional roughness element (such as a wire on the surface) is given by[23]

$$\frac{U_\tau k_{crit}}{\nu} = 7$$

where $U_\tau = (\tau_w/\rho)^{\frac{1}{2}}$ and τ_w is the laminar shear stress at the location of the roughness element. For isolated and distributed point roughness elements, the same parameter appears to apply but the constant is much larger, being in the range 24 to 30[24,25]. Consider the case of a 50 mm diameter cylinder at 90^{o} to the free stream. The maximum laminar shear stress is given by the expression

$$\frac{\tau_w}{\frac{1}{2}\rho U^2} Re_d^{\frac{1}{2}} = 6.36$$

This can be combined with the critical roughness height criteria to give

$$k_{crit} = d \frac{3.93}{Re^{3/4}}$$

for two-dimensional roughness.

and

$$k_{crit} = d \frac{13.5}{Re^{3/4}}$$

for point roughness. At a Reynolds number of 10^5, these two expressions respectively give values of 0.035 mm and 0.12 mm for the critical roughness height. On this basis, only the junction between the nose and the body appears large enough to have any effect. However, while this comparison is helpful as a start in considering the significance of roughness magnitudes, its real relevance is very dubious for two reasons. Firstly, most of the measured roughness is in the form of circumferential grooves produced during the turning of the nose and hence the application of a criterion based on wires orientated perpendicular to the flow is likely to give a considerable over-estimate of the value of k_{crit}. Secondly, and more important, the boundary layer is in reality highly three-dimensional. Unfortunately, there does not appear to be any information on the effect of surface roughness on transition in a three-dimensional boundary layer. A further point is that the action of the surface roughness (if any) may not be to promote transition; indeed, the large range of Reynolds numbers over which roll angle effects have been observed makes it seem quite likely that transition is not the cause of the roll angle effect. On the other hand, it is difficult to think of another mechanism.

The present results do not cover enough points on the model for us to determine whether the variation of $\overline{\Delta C_p}$ with roll angle is due to a change in amplitude of the sectional side force distribution along the body or to a change in its spacing or to a change in both. However, the earlier time-averaged results obtained by Lamont and Hunt[9] showed no change in spacing with roll angle. It will be interesting to see if this behaviour can be confirmed in the R.A.E. tunnel.

4.2.3 Effect of other asymmetries

Certain other limited studies were carried out in the hope of shedding light on the action of asymmetries. In the event, the results deepen the mystery but, since the tests were carefully conducted, the studies are summarised here.

In the first set of these tests, the nose normally used was replaced by an alternative manufactured to the same specifications. In the second set of tests, tape of thickness 0.15 mm was added to the tip of the nose, as shown on Fig. 5. In both cases, measurements of ΔC_p were taken over a range of angles of attack at the station nearest to the first peak of sectional side force for $\alpha < 60^o$ and at the second peak for $\alpha > 60^o$. The Reynolds number was 1×10^5 and the roll angle was set at the datum value.

The mean values of ΔC_p are presented in Fig. 28. It can be seen that both forms of modification to the model have profound effects. However, it is startling that there appears to be no consistency about the nature of the effects: for example, at $\alpha = 60^o$ tape in location "A"

produces an increase in the force but at $\alpha = 40^{o}$, it reduces the force to almost zero. There is little significant variation in the levels of unsteadiness between these various cases.

Further tests were conducted at $\alpha = 50^{o}$ in which the tape was located on the shoulder of the nose (again see Fig. 5). In all cases, the sense of ΔC_p was unchanged from that with the plain nose; tape in location "C" increased $|\overline{\Delta C_p}|$ from 2.23 to 2.27 while in location "D" and simultaneously in locations "C" and "D" the tape caused an increase to 2.52. It thus seems that the pressures are much more sensitive to imperfections near the tip of the nose than they are to imperfections elsewhere, as previously discovered by Keener et al[7].

4.3 Other noses

A limited amount of testing has also been performed on three other noses, all tangent ogives of length 1.0, 2.0 and 2.5 calibres. Most of these tests were performed during the first testing series, using the single Scanco transducer, when the testing technique was still being developed and improvements were being made to the apparatus. Hence the results obtained may be subject to slight inaccuracies in detail, although the general observed trends are believed to be correct.

4.3.1 1.0 calibre ogive nose

The most noticeable result in the traces obtained using the 1.0 calibre tangent ogive nose is that the non-dimensional mean pressure difference $\overline{\Delta C_p}$ is generally quite low for all angles of incidence. The results obtained show some inconsistencies, but this is due partly to the experimental set-up used at the time. Another feature of the results is that in certain of the tests the mean value appeared to be fluctuating at a frequency much lower than that of the unsteadiness normally associated with the pressures measured. An example is shown in Fig. 29 for a test at an incidence of 50^{o}. Figure 30 shows the mean and the amplitude of the unsteady part of the pressures measured and includes data from all the tests performed, although doubts must be cast on the validity of some of the points. Obviously these tests should be repeated more carefully, with the better experimental procedure that has now been developed.

4.3.2 2.0 calibre ogive nose

Tests were carried out using the 2.0 calibre ogive nose during the first test series and although these are reliable, many of the tests were repeated in the latest series using a better experimental technique and it is only these results which are included in this discussion.

Initially, the mean pressure difference measured in the first tests series appeared to be lower than had been anticipated from comparisons with the earlier work of Lamont and Hunt[9]. Having found the large roll angle dependence with the 3.0 calibre nose mentioned earlier, a roll angle survey was performed with the 2.0 calibre nose at an incidence of 50^{o} for varying

Reynolds number. The results are presented in Fig. 31 which shows the mean value $\overline{\Delta C_p}$ against roll angle ϕ and Reynolds number. The figure shows that again there is a roll angle dependence for this nose, and also that changing the Reynolds number produces different results at different roll angles. The two separate tests at $\phi = 180^o$ indicates how repeatable the results were. The amplitude of the unsteadiness did not vary much between the different roll angle tests.

As can be seen in Fig. 31 the maximum mean pressure difference occurs at $\phi = 180^o$, so tests were repeated in the latest series through the incidence range 30^o to 70^o at this roll angle. The results are summarised in Fig. 32. The mean levels are very much lower than those obtained for the 3.0 calibre nose over most of the range, and still are also lower than had been anticipated from Lamont and Hunt's work. The unsteady part of the signals had amplitudes generally slightly less than had been seen on the 3.0 calibre nose, but much less than was obtained in the tests in the Bristol tunnel on the 2.0 calibre nose. Figure 33 shows a comparison between two identical tests in the different tunnels at $\alpha = 50^o$. It is seen that the trace from the R.A.E. tunnel has a reduced amount of unsteadiness and also a lower mean level. This is similar to the comparison made in Fig. 8 for the 3.0 calibre nose at low incidence ($\alpha = 30^o$).

4.3.3 2.5 calibre ogive nose

The only tests performed on this nose were during the early first test series and only a limited number were carried out.

Some of the traces produced were of a very interesting nature. A summary of the results is shown in Fig. 34 which presents the mean level and unsteadiness magnitudes of the signals recorded for all tests performed. It can be seen that there is a discrepancy between the results at the different roll angles at incidence $\alpha = 70^o$. This is because at $\phi = 180^o$ the trace is similar to that for the 3.0 calibre ogive at $\alpha = 70^o$ as shown in Fig. 13(b), with the output "switching" sides with no preferred state (between mean levels of $\overline{\Delta C_p} \simeq \pm 0.95$), whereas at $\phi = 0^o$ the "switching" does not occur so frequently and has a preferred side in which it remains for longer periods, as shown in Fig. 35.

Also of interest are the nature of the traces at incidences of $\alpha = 50^o$ and $\alpha = 60^o$ at each roll angle, because, in these cases, the mean level on the trace fluctuates. In fact at $\alpha = 60^o$, $\phi = 180^o$ there is a tendency for the trace to "switch" occasionally towards its mirror image state as shown in Fig. 36.

It is noteworthy that the mean levels shown in Fig. 34 depart from zero and reach a peak at higher incidences than for any other noses, although the measuring stations were chosen using the same principles, as near as possible to a peak in the time-averaged side force distribution given in the paper of Lamont and Hunt[9]. This implies that the sectional side force developed on the body fitted with the 2.5 calibre ogive nose starts to develop

at higher incidence and remains present at higher incidence than was found on any of the other noses. Clearly more investigation needs to be done into these very interesting results.

5. CONCLUSIONS

The two most important findings in this work are as follows:

(1) The surface pressures on a rigidly clamped model are vastly more steady in a stream of turbulence level equal to 0.01% than they are in a stream of turbulence level 0.7%. Meaningful time-averaged data for the side force are therefore unlikely to be obtained in test conditions where the turbulence level is moderate or high.

(2) The surface pressures are dependent on roll angle even in the low turbulence level stream. The mechanism for this is unknown at present but the implication is clear: even strict control of the free stream conditions is not sufficient to guarantee results which are independent of the experimental equipment.

The following conclusions can also be drawn:

(3) Some inherent unsteadiness exists in the flow pattern but is unlikely to prevent the acquisition of reliable time-averaged measurements. The unsteadiness has the form of classical Karman vortex shedding at very high angles of attack and far from the nose at lower angles of attack.

(4) No correlation could be found between isolated blemishes or surface roughness on the nose of the model and the measured variation with roll angle.

(5) Fitting an alternative nose or adding tape to the nose tip produced large changes in the surface pressures but in a manner which varied with angle of attack.

(6) The addition of tape to the shoulder produced relatively little effect, thus confirming the observations of Keener et al[7].

(7) While remaining in the subcritical region an increase in Reynolds number causes little change to the mean level or amplitude of the unsteadiness of the measured non-dimensional pressure difference.

(8) The most self-consistent set of results was obtained with a three calibre nose. Shorter noses showed the same reduced unsteadiness with reduced turbulence level as did the three calibre nose. However, they gave rise to lower mean pressures and interpreting the results was more difficult. A more careful examination of the pressures associated with the shorter noses is desirable when the influence of roll angle has been properly understood.

6. LITERATURE CITED

1. LETKO, W., "A low-speed experimental study of the directional characteristics of a sharp-nosed fuselage through a large angle of attack range at zero angle of side slip", NACA, 1953, TN2911.

2. DUNN, E.L., "A low-speed experimental study of yaw forces on bodies of revolution at large angles of pitch and zero angle of side slip", U.S. Naval Ordnance Test Station, China Lake, Calif., 1954, TM1588.

3. NIELSEN, J.N., "Non-linearities in missile aerodynamics", AIAA Paper 78-20, 1978.

4. AIAA, 4th Atmospheric Flight Mechanics Conference, Hollywood, Florida, August 8-10, 1977.

5. AIAA, 16th Aerospace Sciences Meeting, Huntsville, Alabama, January 16-18, 1978.

6. WARDLAW, A.B. and MORRISON, A.M., "Induced side forces at high angles of attack", J. Spacecraft, Vol. 13, No. 10, 1976, 589-593.

7. KEENER, E.R., CHAPMAN, G.T., COHEN, L. and TALEGHANI, J., "Side forces on a tangent ogive forebody with a fineness ratio of 3.5 at high angles of attack and Mach Numbers from 0.1 to 0.7", NASA, 1977, TM X-3437.

8. KEENER, E.R., CHAPMAN, G.T., COHEN, L. and TALEGHANI, J., "Side forces on forebodies at high angles of attack and Mach Numbers from 0.1 to 0.7: two tangent ogives, paraboloid and cone", NASA, 1977, TM X-3438.

9. LAMONT, P.J. and HUNT, B.L., "Pressure and force distributions on a sharp-nosed circular cylinder at large angles of inclination to a uniform, subsonic stream", J. Fluid Mechanics, Vol. 76, Part 3, 1976, 519-559.

10. LAMONT, P.J. and HUNT, B.L., "Prediction of aerodynamic out-of-plane forces on ogive-nosed circular cylinders", J. Spacecraft, Vol. 14, No. 1, 1977, 38-44.

11. LAMONT, P.J. and HUNT, B.L., "Comment on induced side forces at high angle of attack", J. Spacecraft, Vol. 14, No. 5, 1977,319.

12. CLARK, W., "Body vortex formation on missiles in incompressible flows", AIAA Paper 77-1154, 1977.

13. COE, P.L., CHAMBERS, J.R. and LETKO, W., "Asymmetric lateral-direction characteristics of pointed bodies of revolution at high angles of attack", NASA, 1972, TND-7095.

14. BOSTOCK, B.R., "Slender bodies of revolution at incidence", University of Cambridge, 1972, Ph.D. Thesis.

15. SQUIRE, H.B. and WINTER, K.G., "The R.A.E. 4 ft x 3 ft experimental low turbulence wind tunnel", Part I, A.R.C., 1948, R & M 2690.

16. SCHUH, H. and WINTER, K.G., "The R.A.E. 4 ft x 3 ft experimental low turbulence wind tunnel", Part II, A.R.C., 1957, R & M 2905.

17. SCHUH, H. and WINTER, K.G., "The R.A.E. 4 ft x 3 ft experimental low turbulence wind tunnel", Part IV, A.R.C., 1962, R & M 3261.

18. HUNT, B.L. and DEXTER, P.C., "Pressures on a slender body at high angle of attack in a very low turbulence level air stream", to be presented at AGARD Symposium on High Angle of Attack Aerodynamics, Sandefjord, Norway, 4-6 October 1978.

19. LAMONT, P.J., "The out-of-plane force on an ogive-nosed cylinder at large angles of inclination to a uniform stream", University of Bristol, Ph.D. Thesis, 1973.

20. BRYAN, M.J. and WALSH, B.J., "An investigation into the low frequency response of pressure tubing used in wind tunnel experimentation", B.Sc., Bristol University, 1975, Undergraduate Report No. 193.

21. REDING, J.P. and ERICSSON, L.E., "Maximum vortex-induced side forces on slender bodies, AIAA Paper 77-1155, 1977.

22. CLARKSON, M.H., MALCOLM, G.N. and CHAPMAN, G.T., "A subsonic, high angle-of-attack flow investigation at several Reynolds Numbers", AIAA, Vol. 16, No. 1, 1978, 53-60.

23. SCHLICHTING, H., Boundary Layer Theory, 4th Edition, New York, McGraw-Hill, 1960, 445-451.

24. TANI, I., "Effect of two-dimensional and isolated roughness on laminar flow", G.V. Lachmann (Ed.)., Boundary Layer and Flow Control, Vol. 2, Pergamon, 1961, 637-656.

25. VON DOENHOFF, A.E. and BRASLOW, A.L., "The effect of distributed surface roughness on laminar flow", G.V. Lachmann (Ed.), Boundary Layer and Flow Control, Vol. 2, Pergamon, 1961, 657-681.

7. GLOSSARY

a	Speed of sound
d	Diameter of cylinder
k_{crit}	Minimum height of roughness to promote transition
Re	Reynolds number, $Ud\,\mathrm{cosec}\alpha/\nu$
p'	Fluctuating pressure
U	Free stream velocity
u'	Fluctuating velocity
U_τ	Friction velocity $(\tau_w/\rho)^{\frac{1}{2}}$
x	Axial distance measured from tip of nose
α	Angle of attack
ΔC_p	Coefficient of pressure difference based on cross flow dynamic head, $\Delta p/\frac{1}{2}\rho U^2 \sin^2\alpha$
$\Delta C_p'$	Amplitude of fluctuations of pressure difference coefficient
$\overline{\Delta C_p}$	Mean value of pressure difference coefficient
Δ_p	Difference between surface pressures at points $\pm\,\theta$ from leading generator
θ	Angle around body from the leading generator
ρ	Density
ϕ	Roll angle
τ_w	Wall shear stress

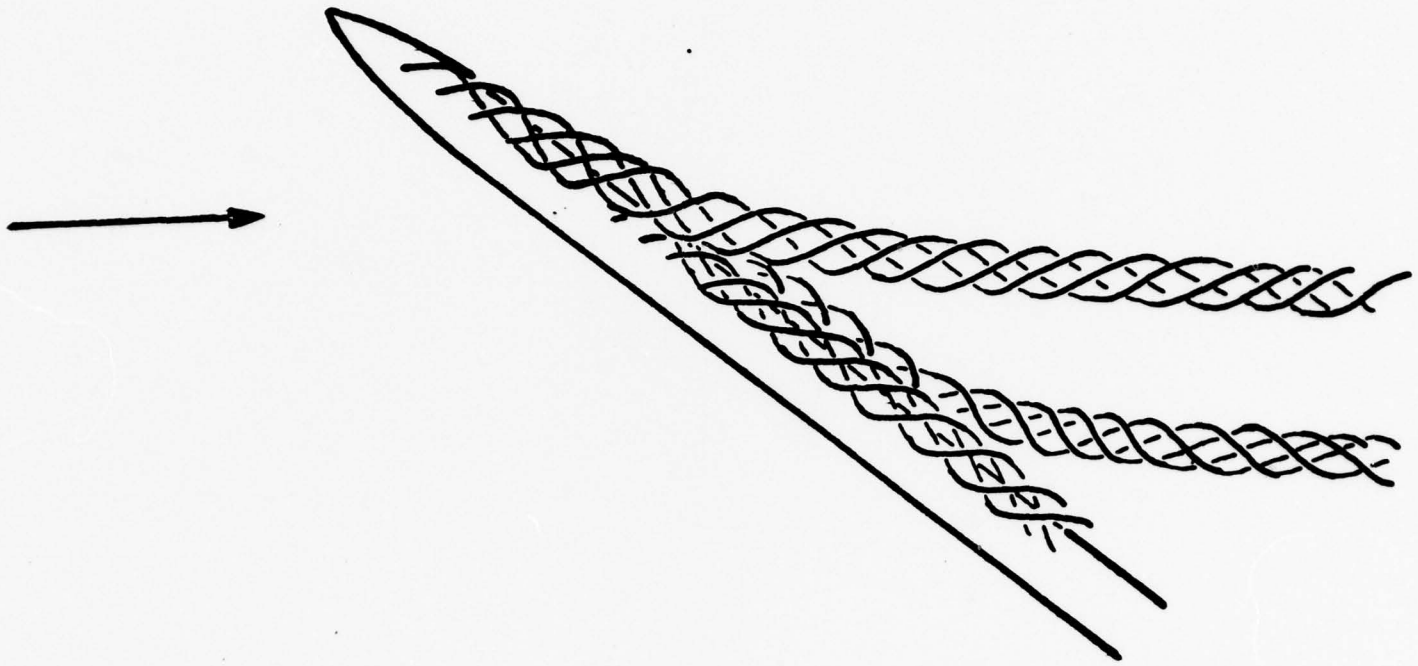

Fig. 1 Sketch of idealised wake vortex pattern

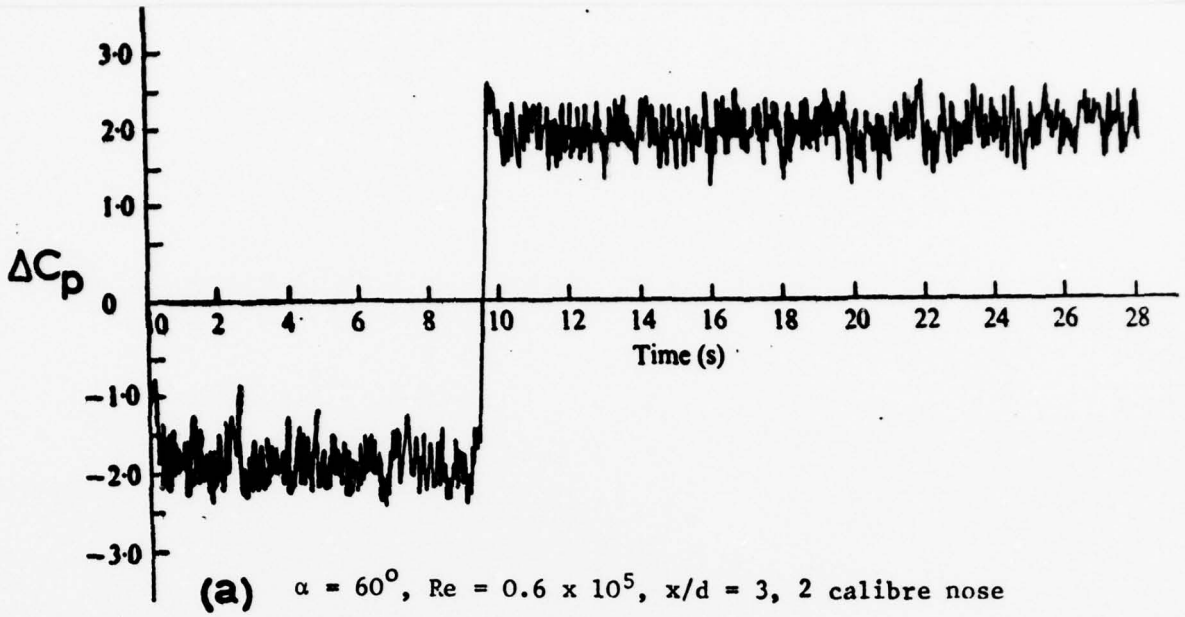

(a) $\alpha = 60^{\circ}$, $Re = 0.6 \times 10^5$, $x/d = 3$, 2 calibre nose

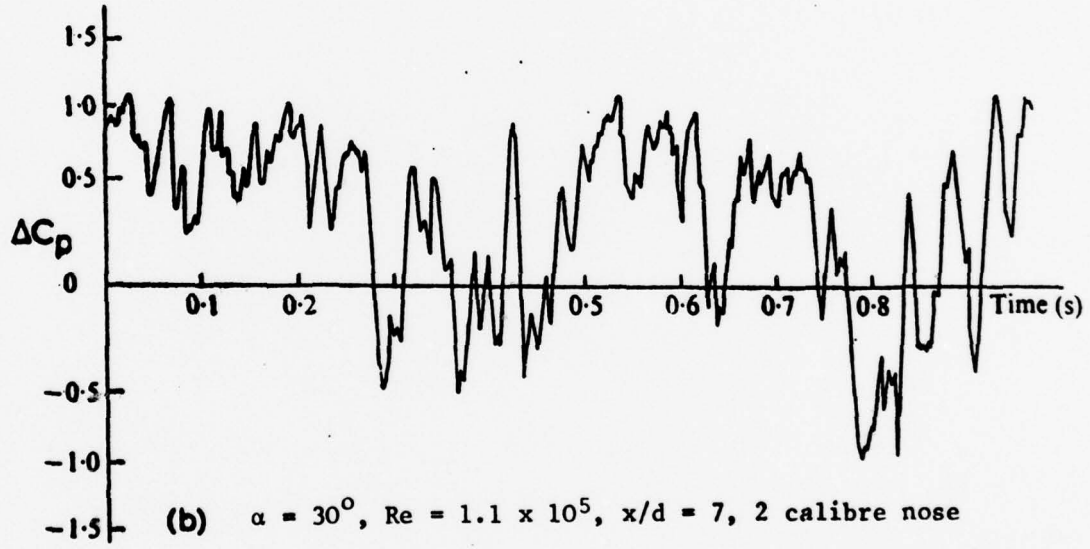

(b) $\alpha = 30^{\circ}$, $Re = 1.1 \times 10^5$, $x/d = 7$, 2 calibre nose

Fig. 2 Time dependent pressure differences recorded by Lamont and Hunt[9]

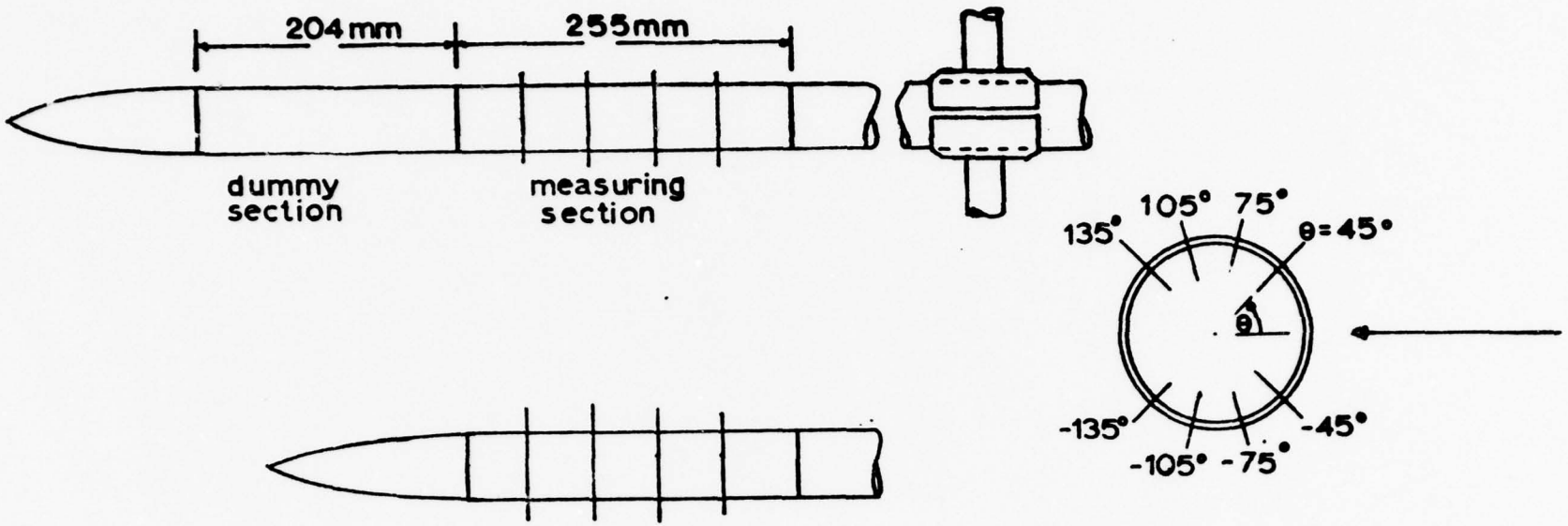

Fig. 3 Sketch of wind tunnel model

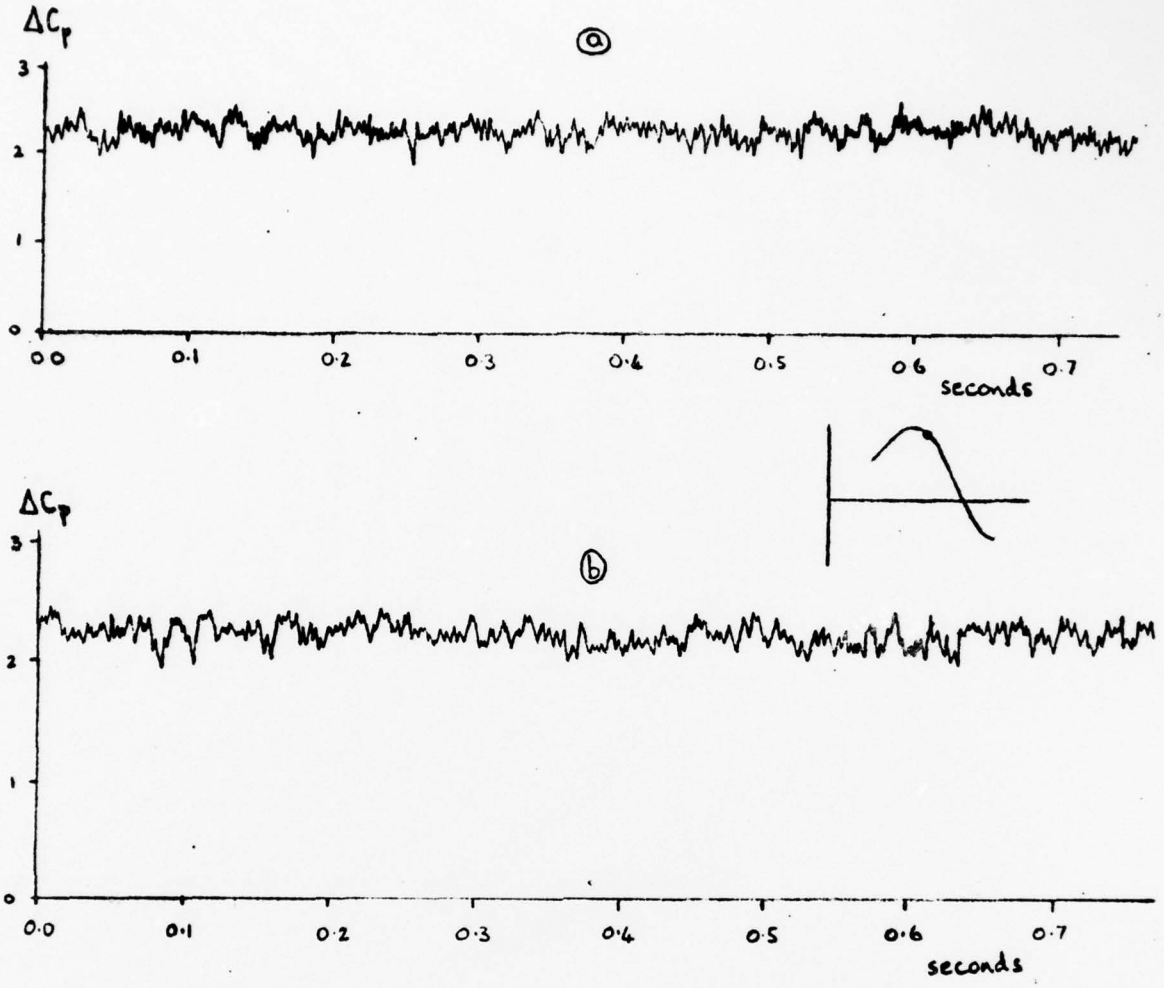

Fig. 4 Comparison of traces from R.A.E. tunnel using (a) 1 Scanco and (b) 2 Setra transducers

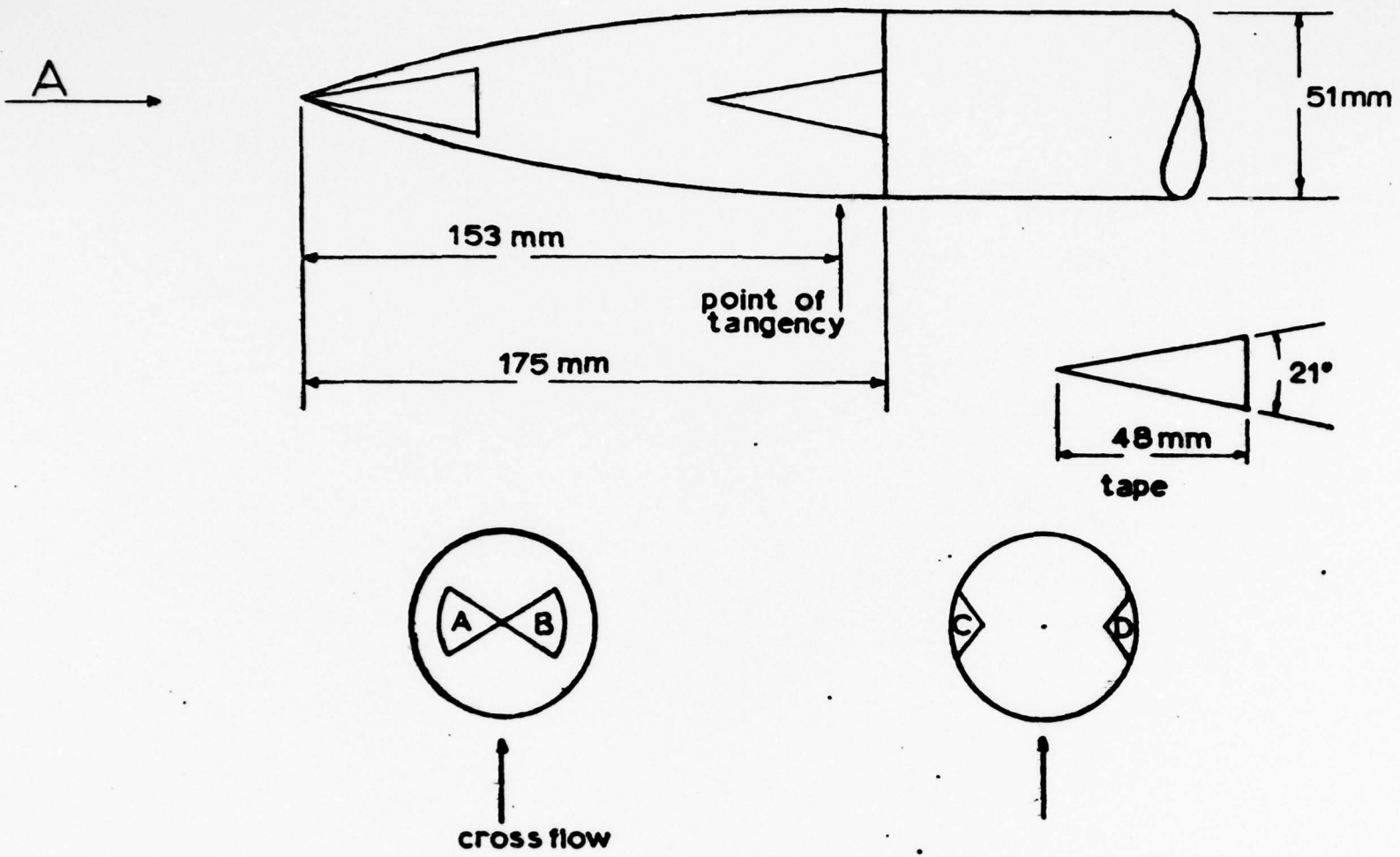

Fig. 5 Location on nose of plastic tape of thickness 0.15 mm

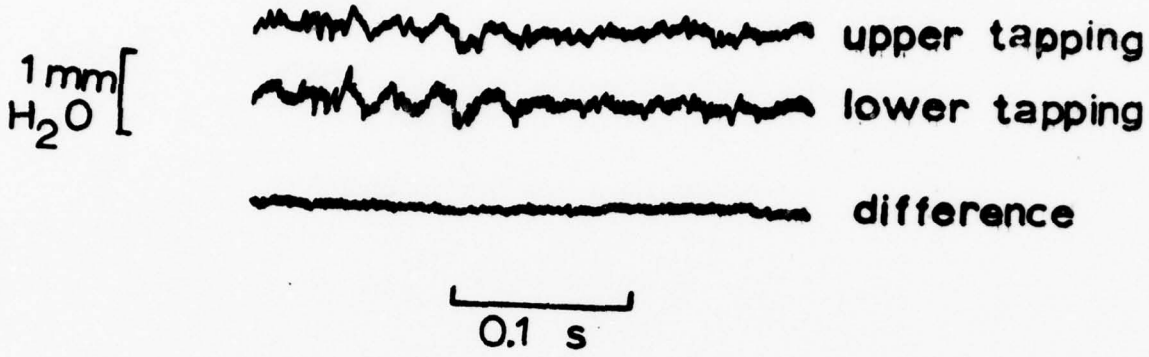

Fig. 6 Transient pressures for $\alpha = 0^{\circ}$, $x/d = 5$, $U = 30$ m/s

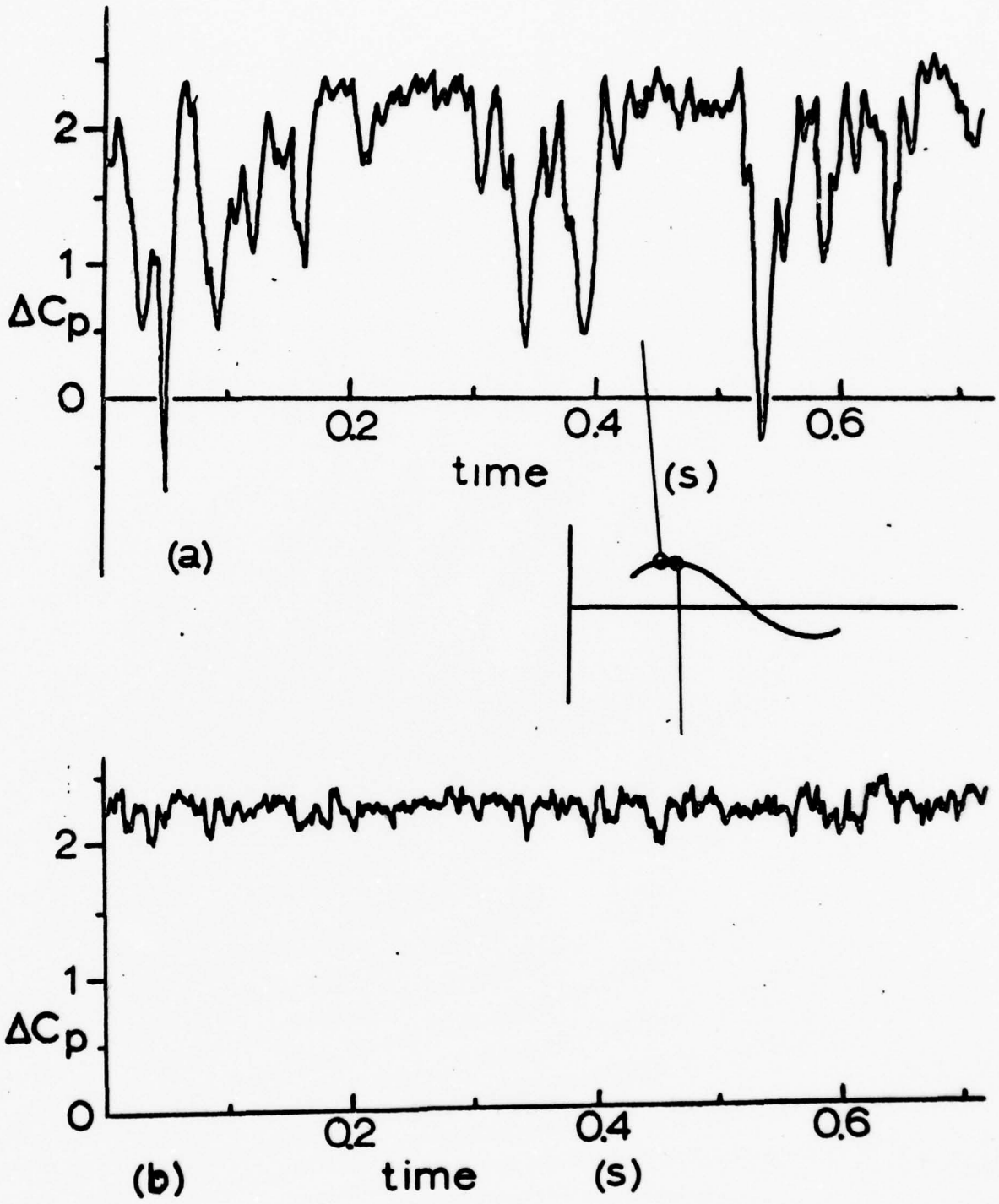

Fig. 7 Transient pressure differences for $\alpha = 50^{\circ}$, Re = 1.1 x 10
(a) Bristol tunnel, x/d = 4; (b) R.A.E. tunnel, x/d = 5

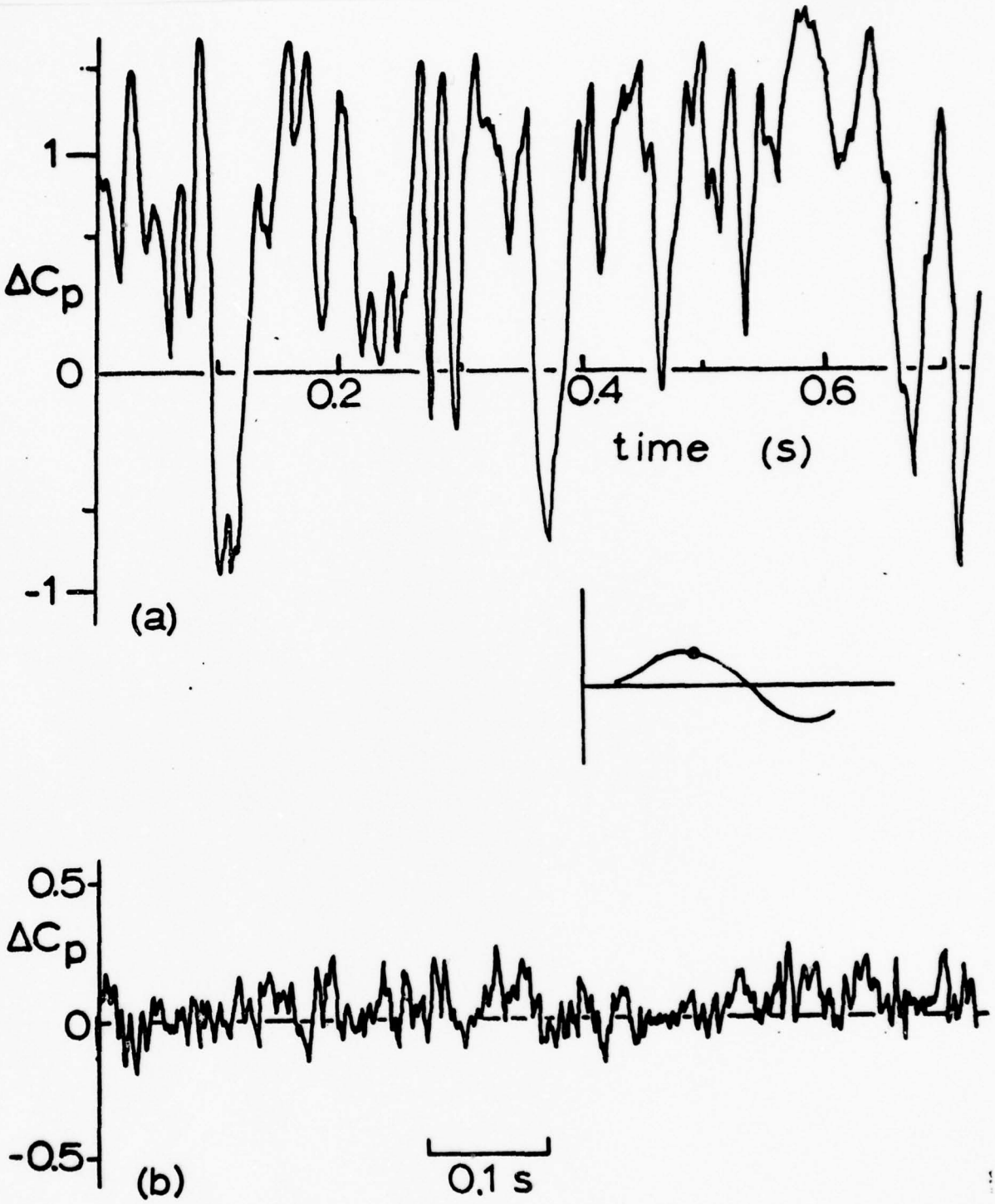

Fig. 8 Transient pressure differences for $\alpha = 30^{o}$, Re = 1.1×10^{5}, x/d = 8; (a) Bristol tunnel; (b) R.A.E. tunnel

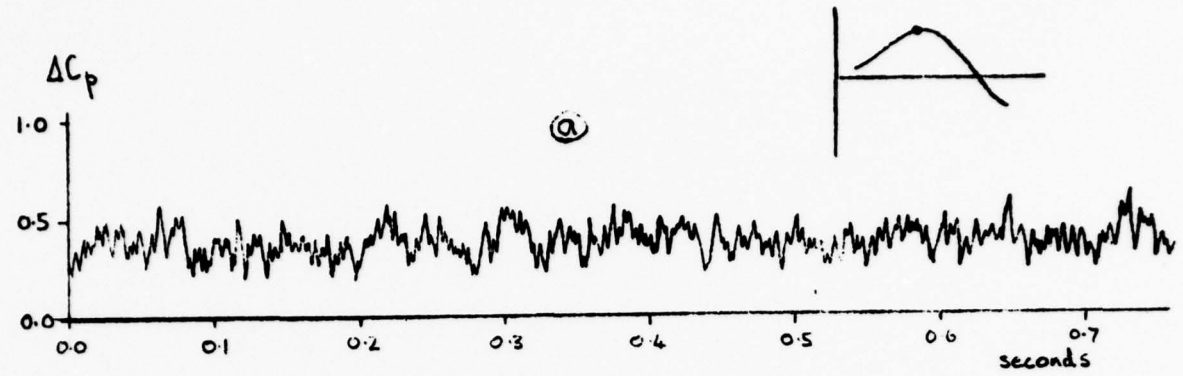

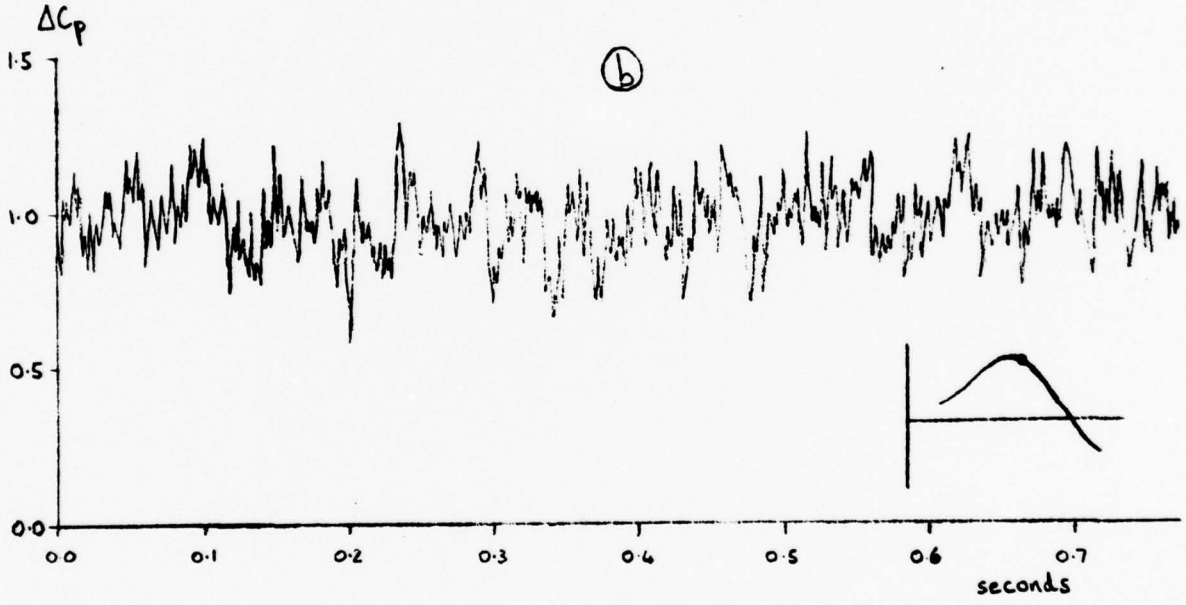

Fig. 9 Transient pressure differences in R.A.E. tunnel, Re = 1.0 x 10^5; (a) $\alpha = 35^0$, x/d = 7; (b) $\alpha = 40^0$, x/d = 7

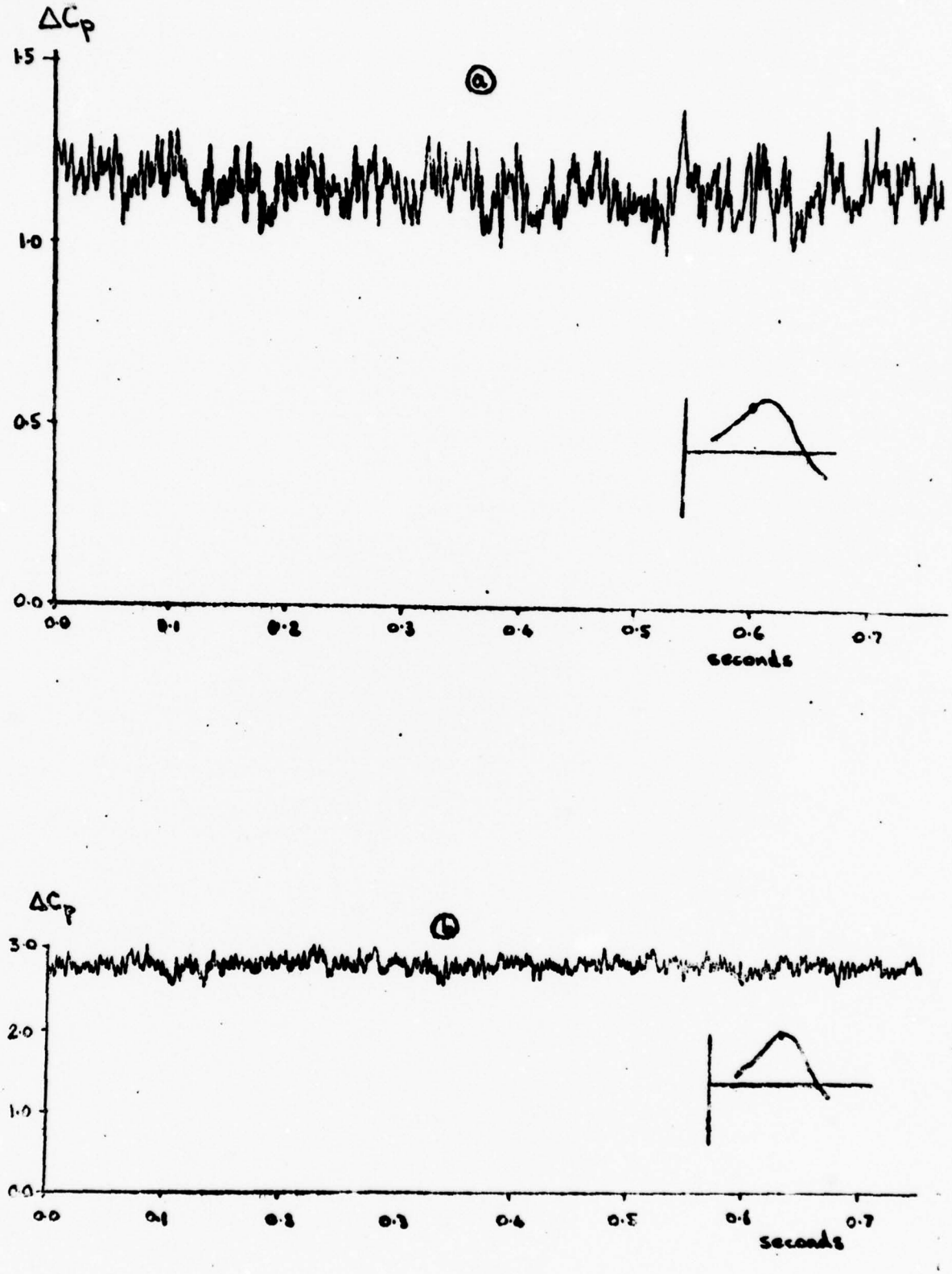

Fig. 10 Transient pressure differences in R.A.E. tunnel, Re = 1.0×10^5; (a) $\alpha = 45^\circ$, x/d = 5; (b) $\alpha = 55^\circ$, x/d = 4

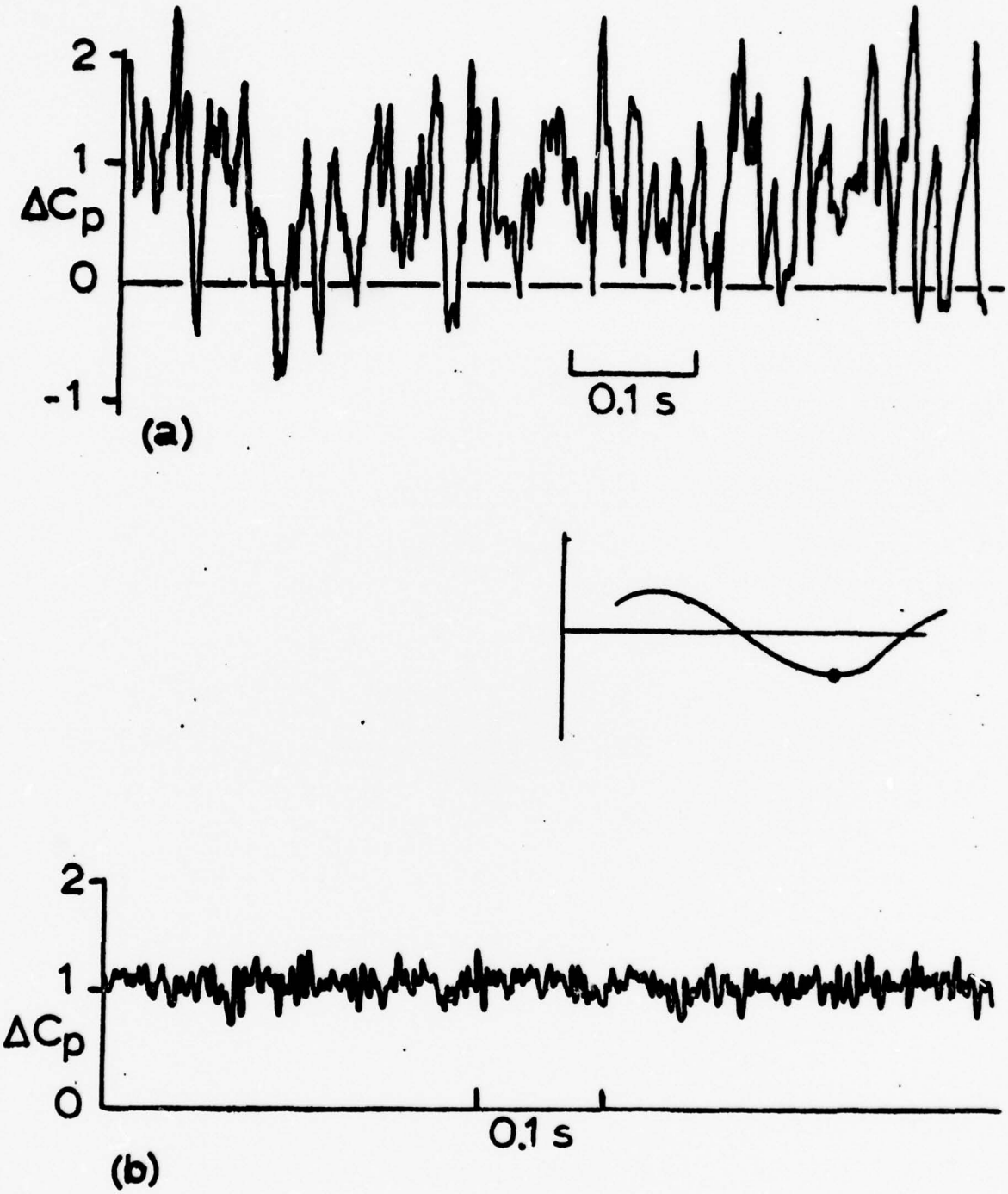

Fig. 11 Transient pressure differences for $\alpha = 60^{\circ}$, $Re = 1.1 \times 10^{5}$, $x/d = 5$; (a) Bristol tunnel; (b) R.A.E. tunnel

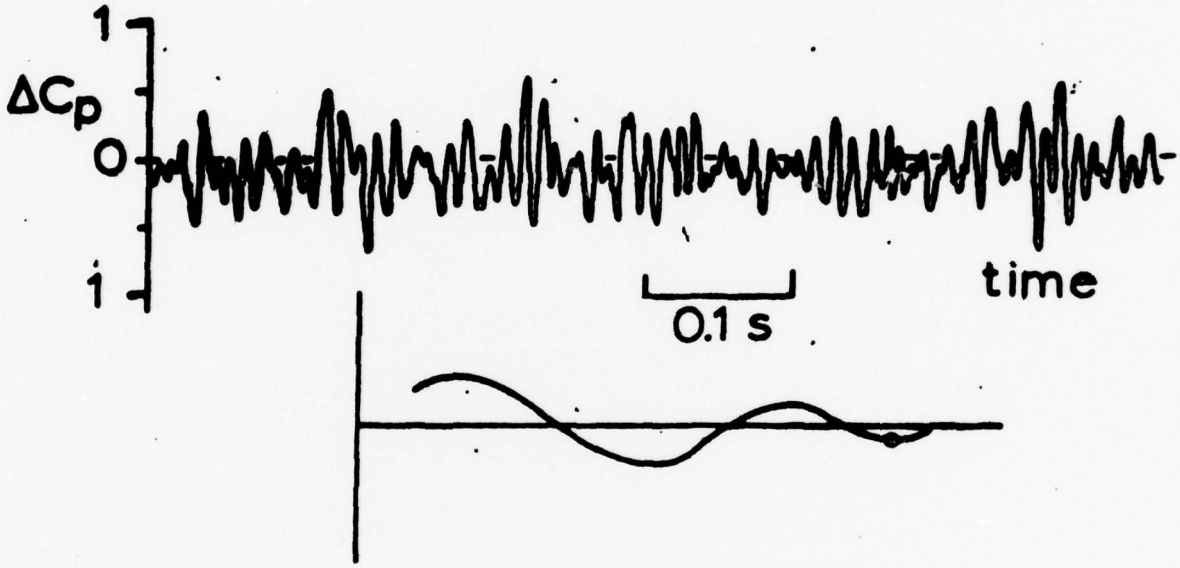

Fig. 12 **Transient pressure difference in R.A.E. tunnel for $\alpha = 60^{o}$; Re = 1.0 x 10^{5}, x/d = 11.**

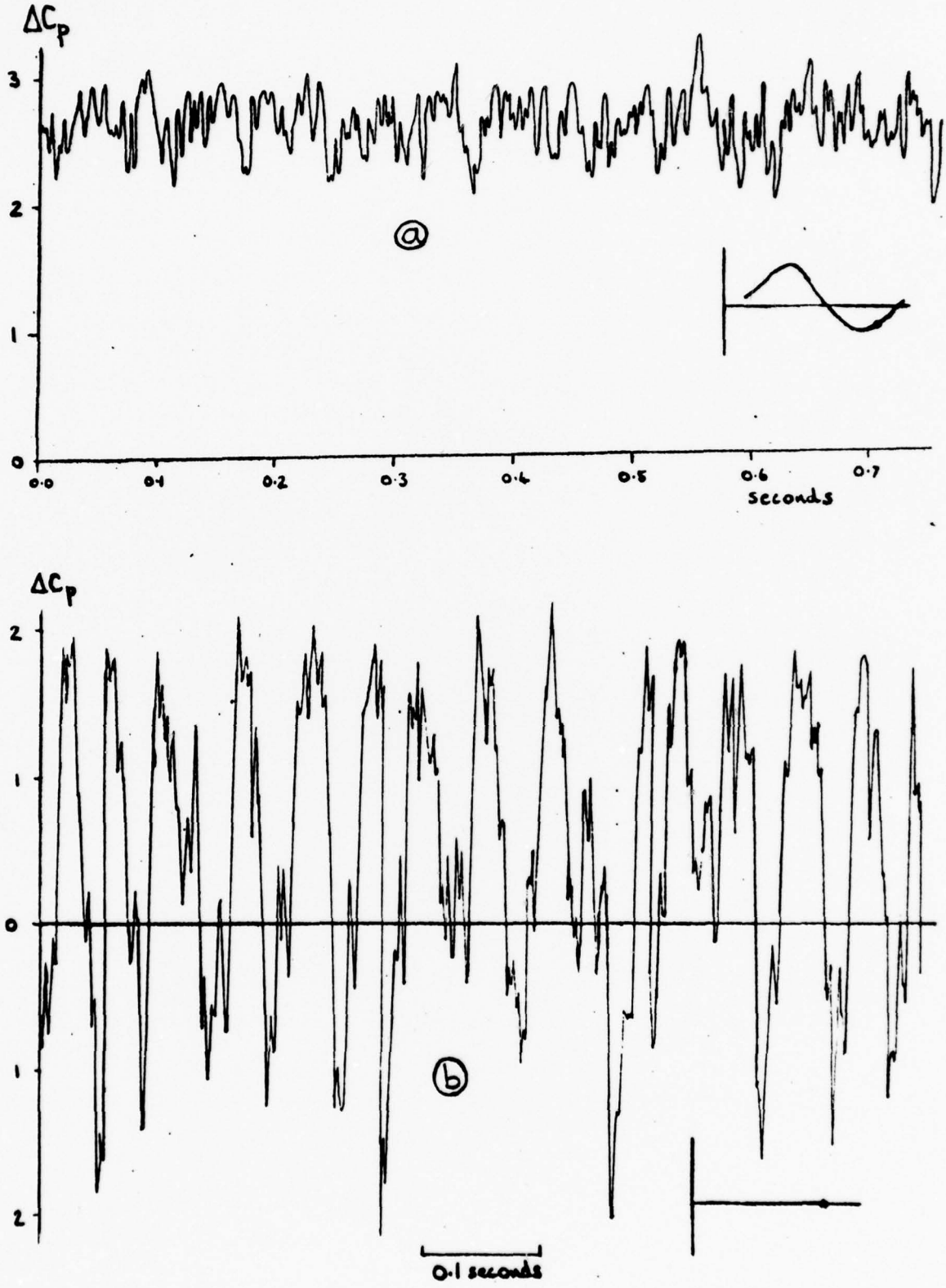

Fig. 13 Transient pressure differences in R.A.E. tunnel, Re = 1.0 x 10^5; (a) $\alpha = 65^0$, x/d = 4; (b) $\alpha = 70^0$, x/d = 4

Fig. 14 Transient pressure difference in R.A.E. tunnel for $\alpha = 75^{\circ}$, $Re = 1.0 \times 10^5$, $x/d = 5$

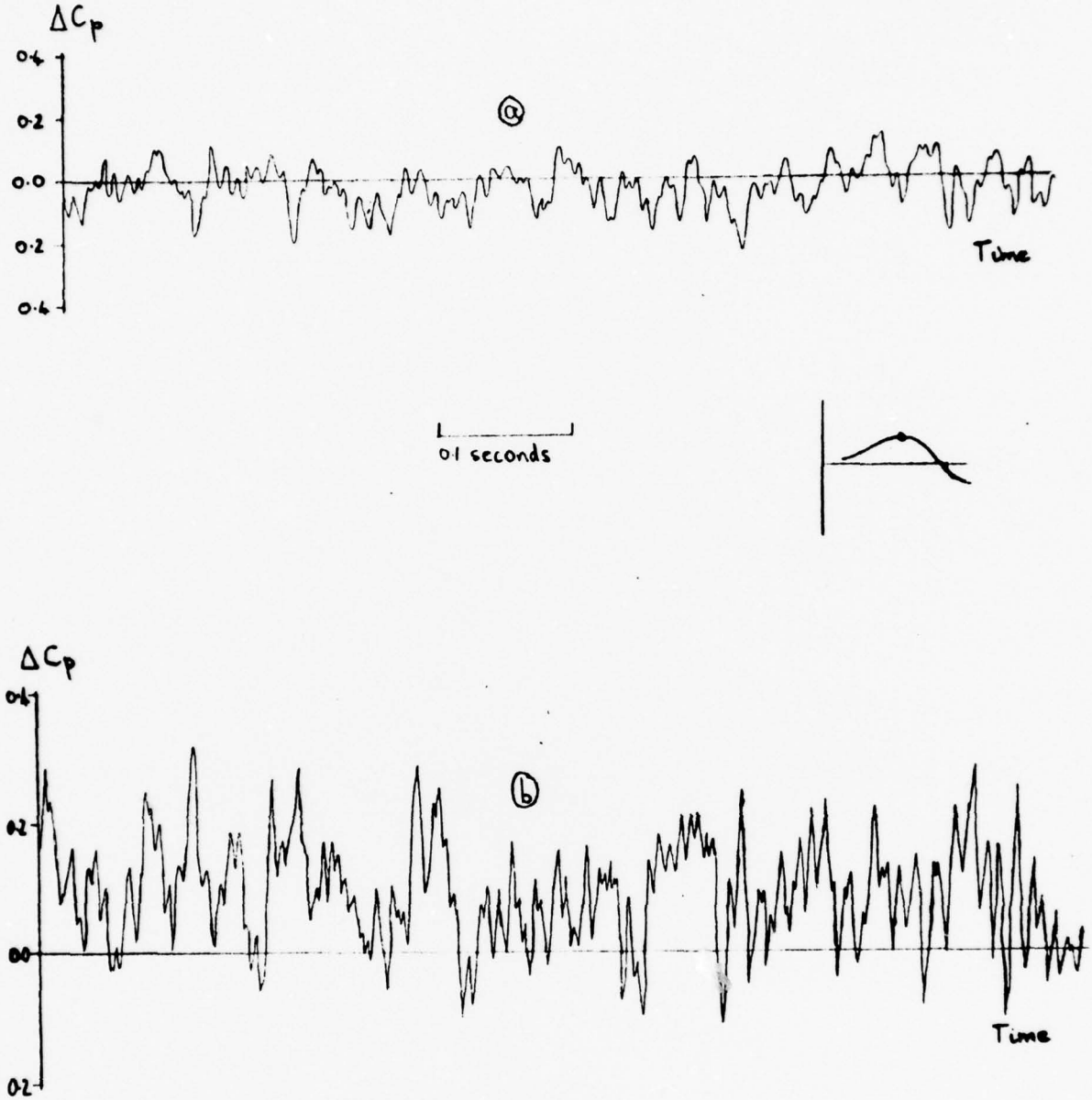

Fig. 15 Transient pressure differences for $\alpha = 30^{o}$, x/d = 8; (a) Re = 0.7 x 10^5; (b) Re = 1.0 x 10^5

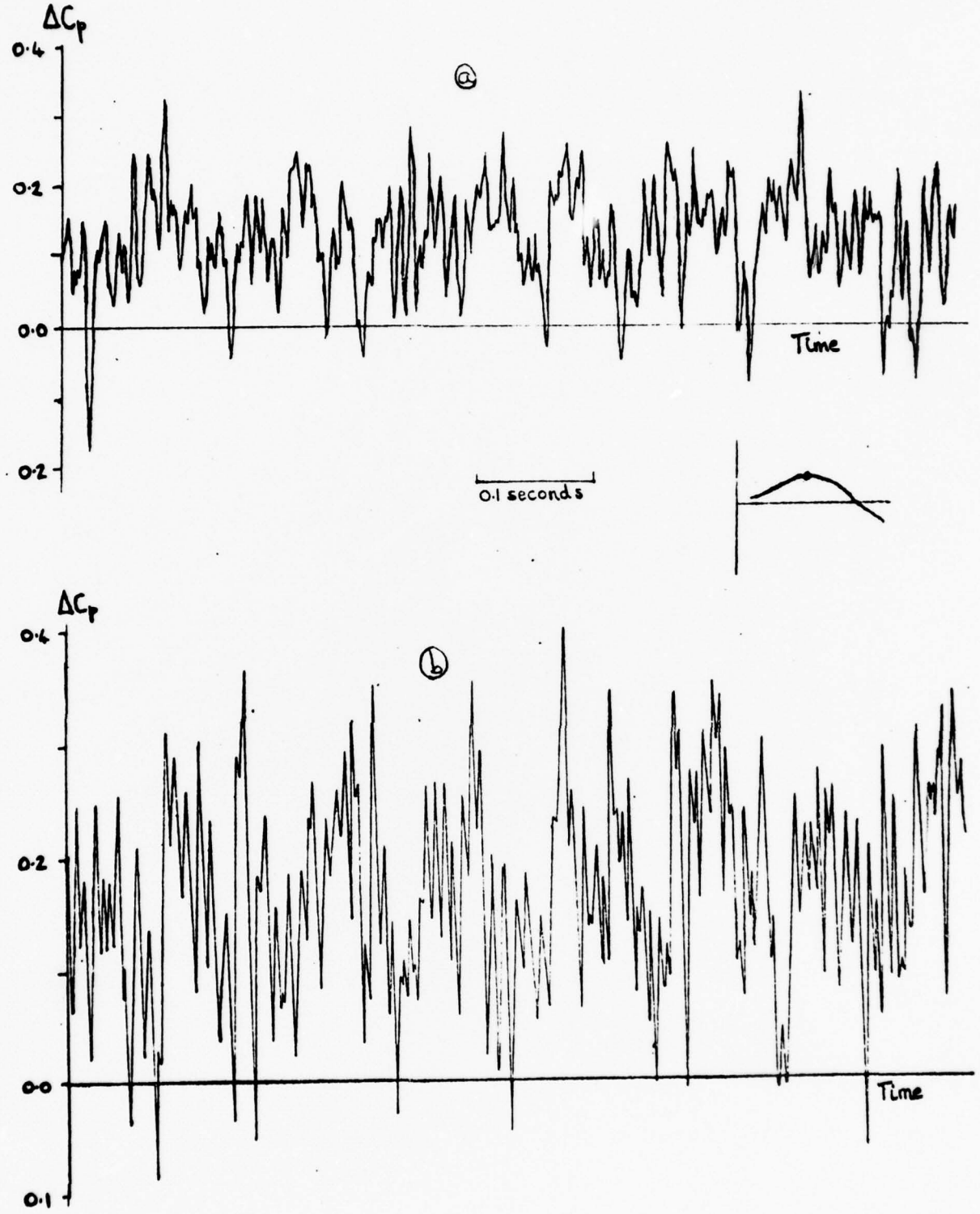

Fig. 16 Transient pressure differences for $\alpha = 30^{o}$, x/d = 8;
(a) Re = 1.1×10^{5}; (b) Re = 1.4×10^{5}

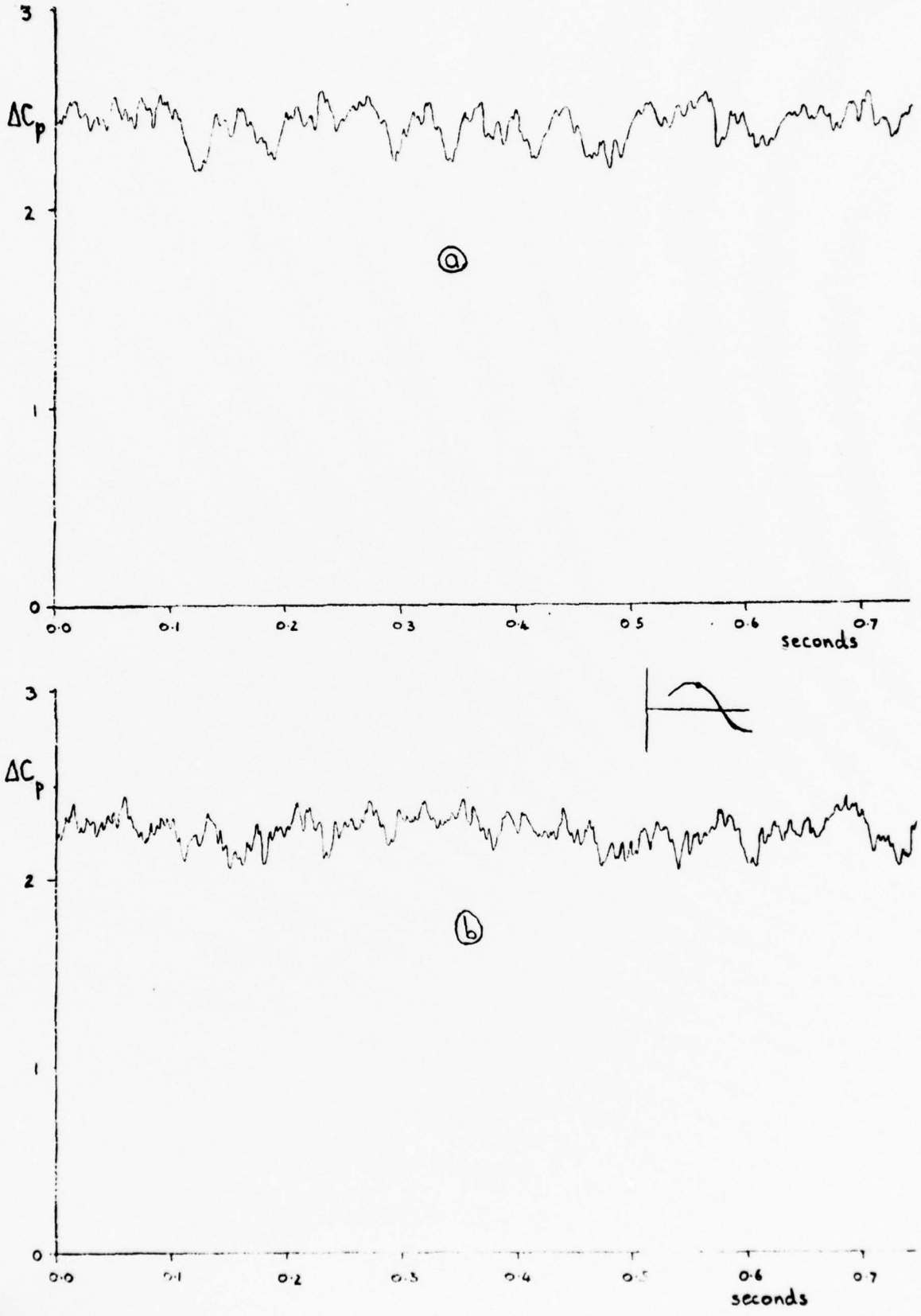

Fig. 17 Transient pressure differences for $\alpha = 50^{\circ}$, x/d = 5;
(a) Re = 0.5×10^5; (b) Re = 0.7×10^5

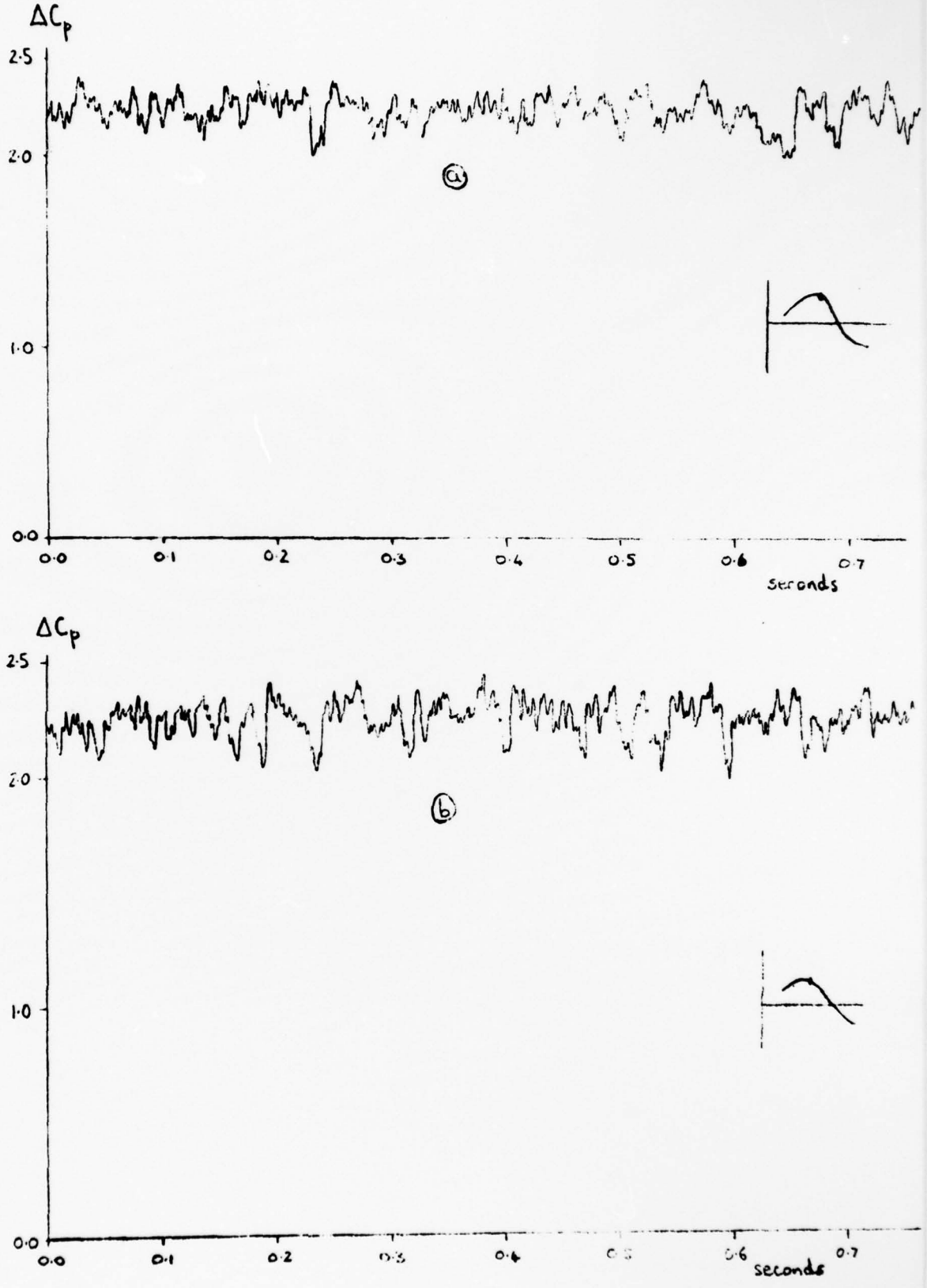

Fig. 18 Transient pressure differences for $\alpha = 50^{\circ}$, x/d = 5;
(a) Re = 1.0×10^5; (b) Re = 1.1×10^5

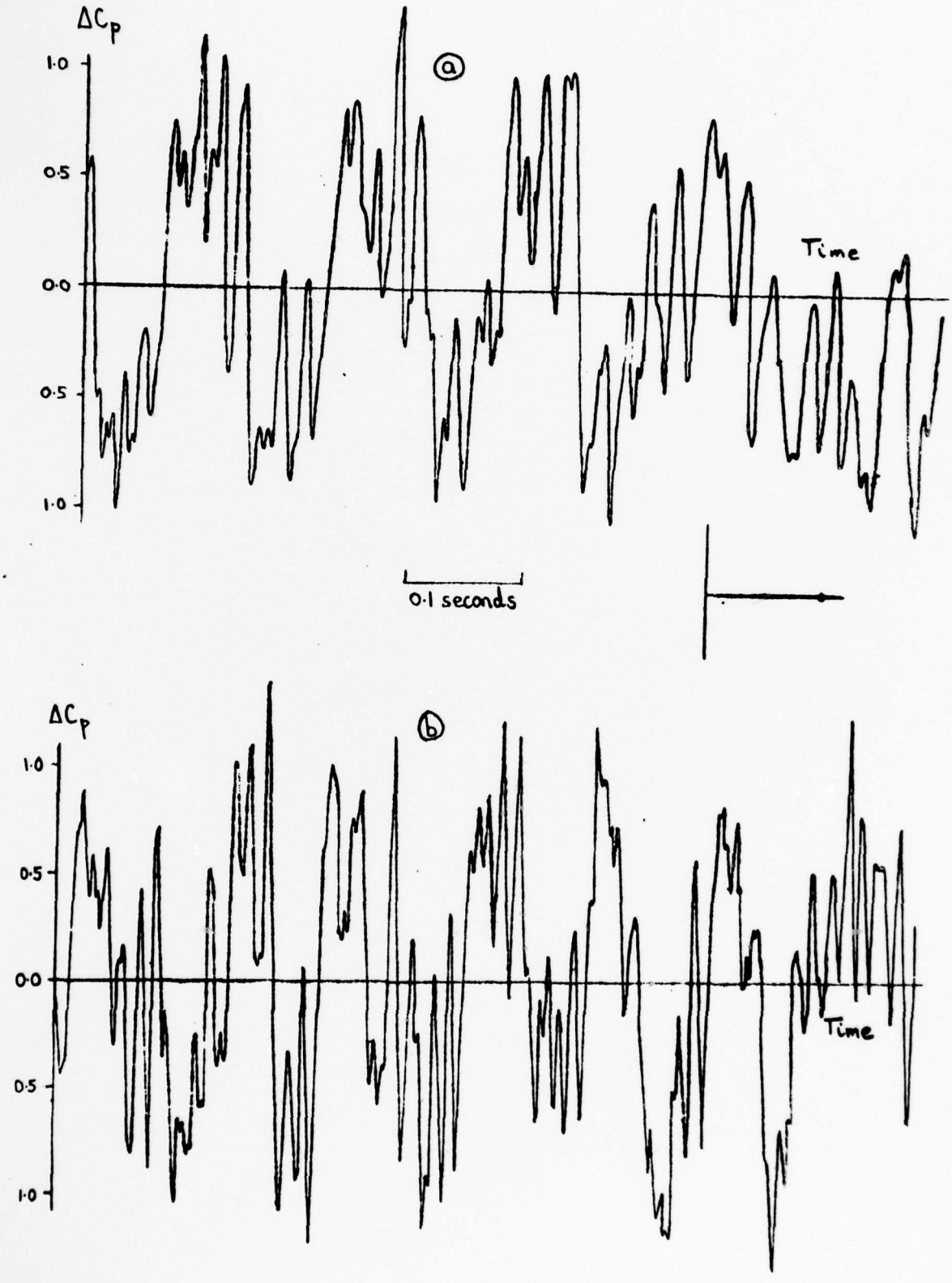

Fig. 19 Transient pressure differences for $\alpha = 70^{o}$, $x/d = 5$;
(a) $Re = 0.5 \times 10^{5}$; (b) $Re = 0.7 \times 10^{5}$

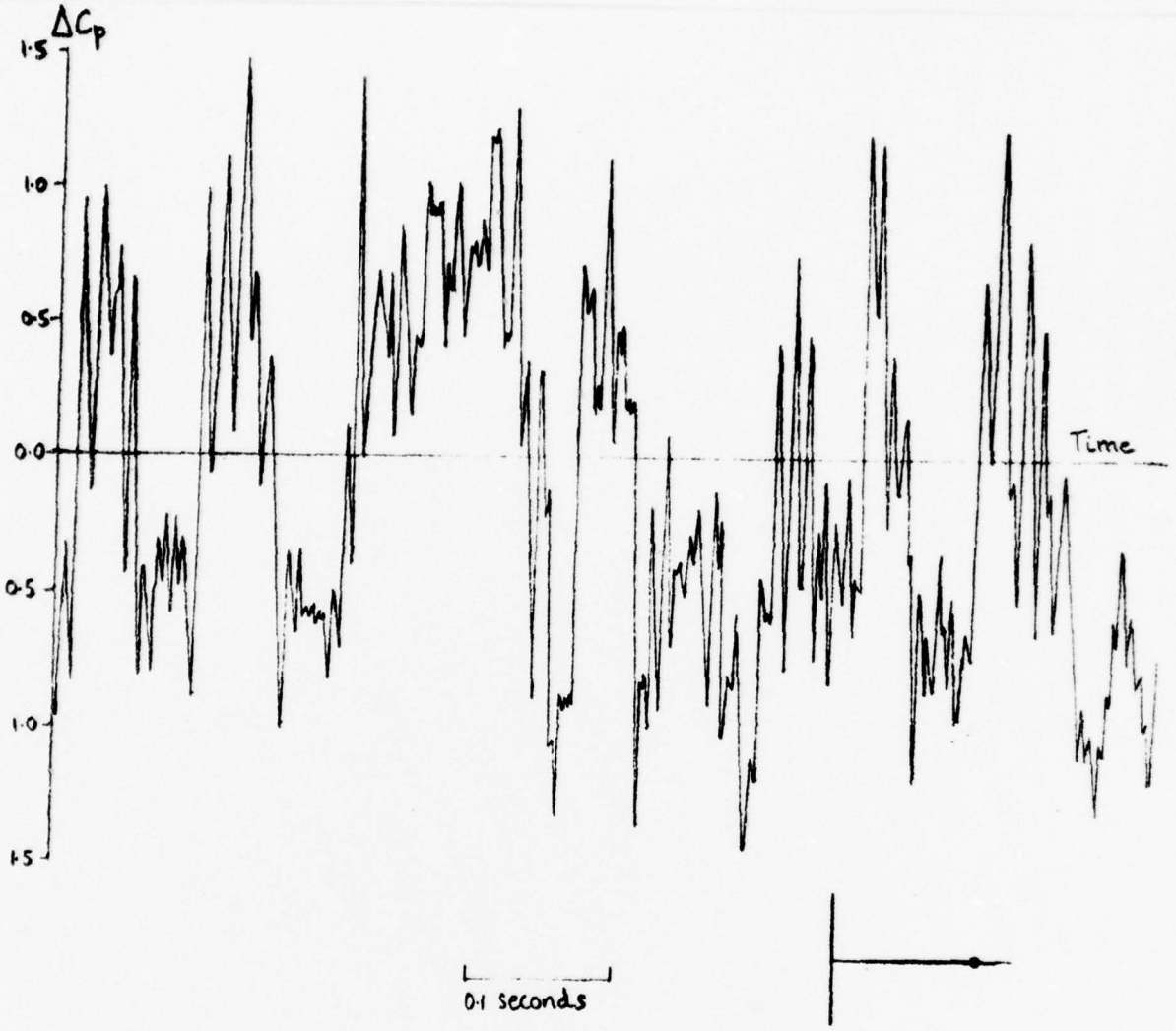

Fig. 20 Transient pressure difference for $\alpha = 70^{o}$, x/d = 5, Re = 1.0 x 10^{5}

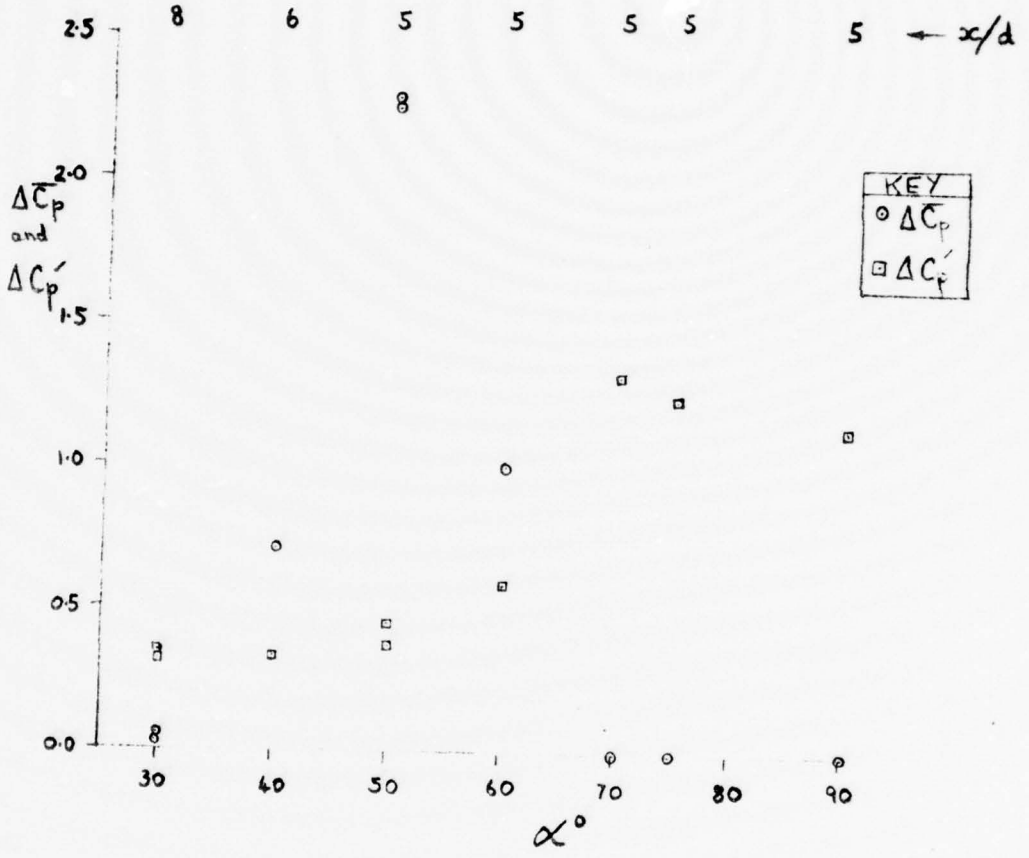

Fig. 21 Variation of mean and of amplitude of fluctuating pressure differences with incidence at Re = 0.7×10^5

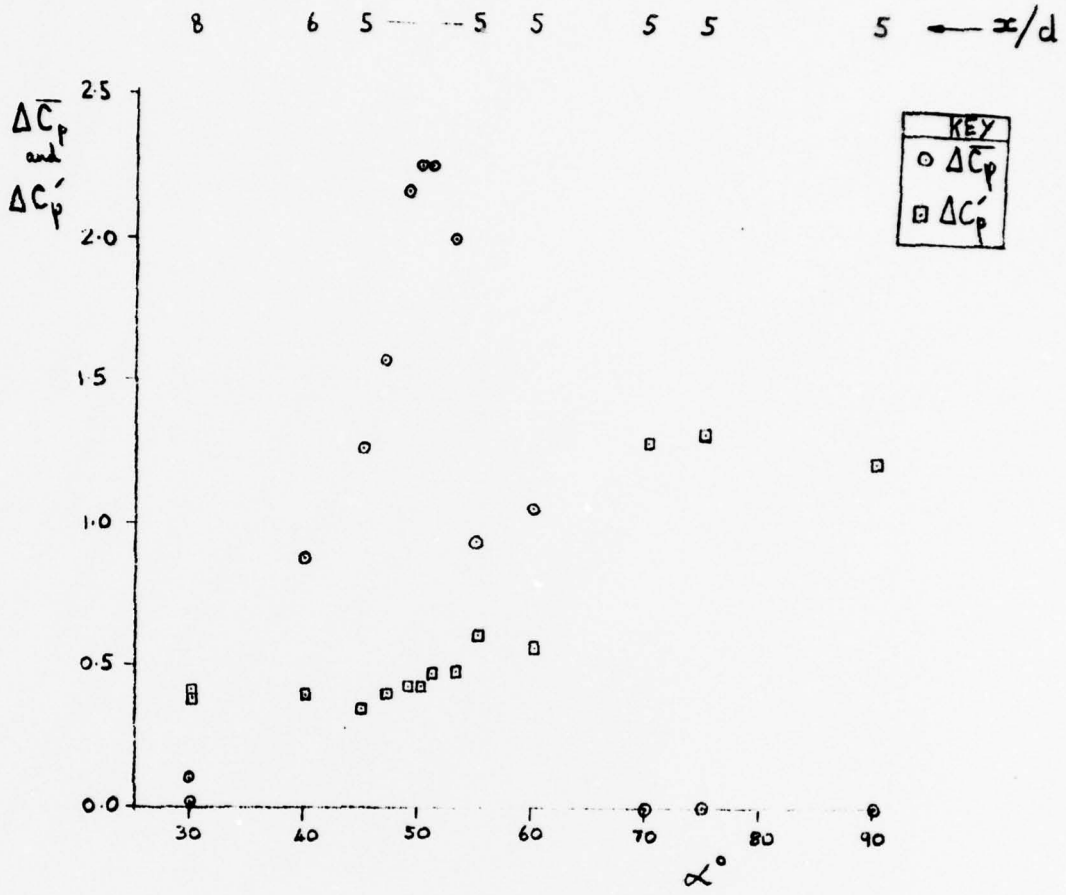

Fig. 22 Variation of mean and of amplitude of fluctuating pressure differences with incidence at Re = 1.0×10^5

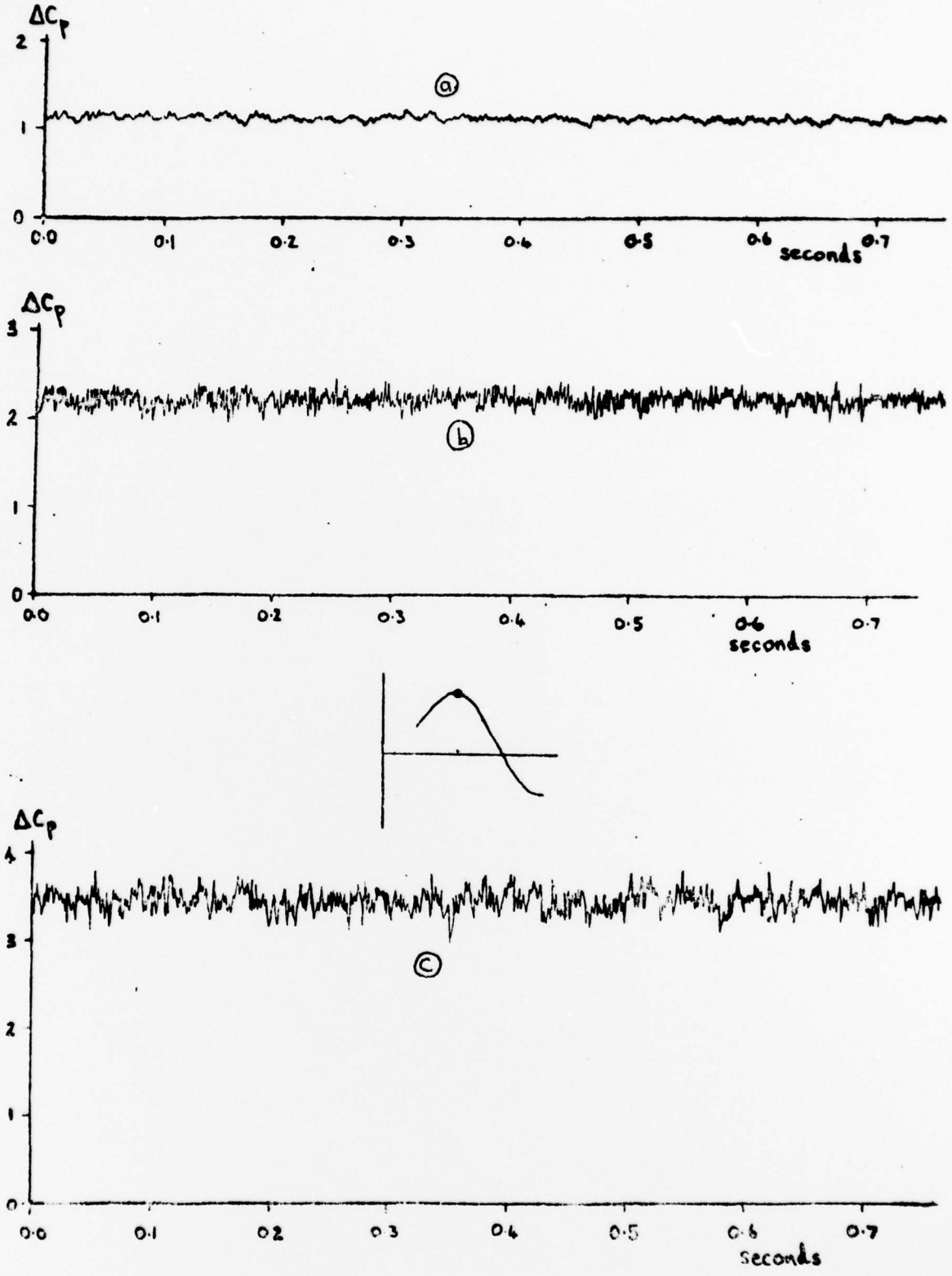

Fig. 23 Transient pressure differences for $\alpha = 55^{\circ}$, $x/d = 4$, $Re = 1.0 \times 10^5$; (a) $\theta = \pm 45^{\circ}$; (b) $\theta = \pm 105^{\circ}$; (c) $\theta = \pm 135^{\circ}$

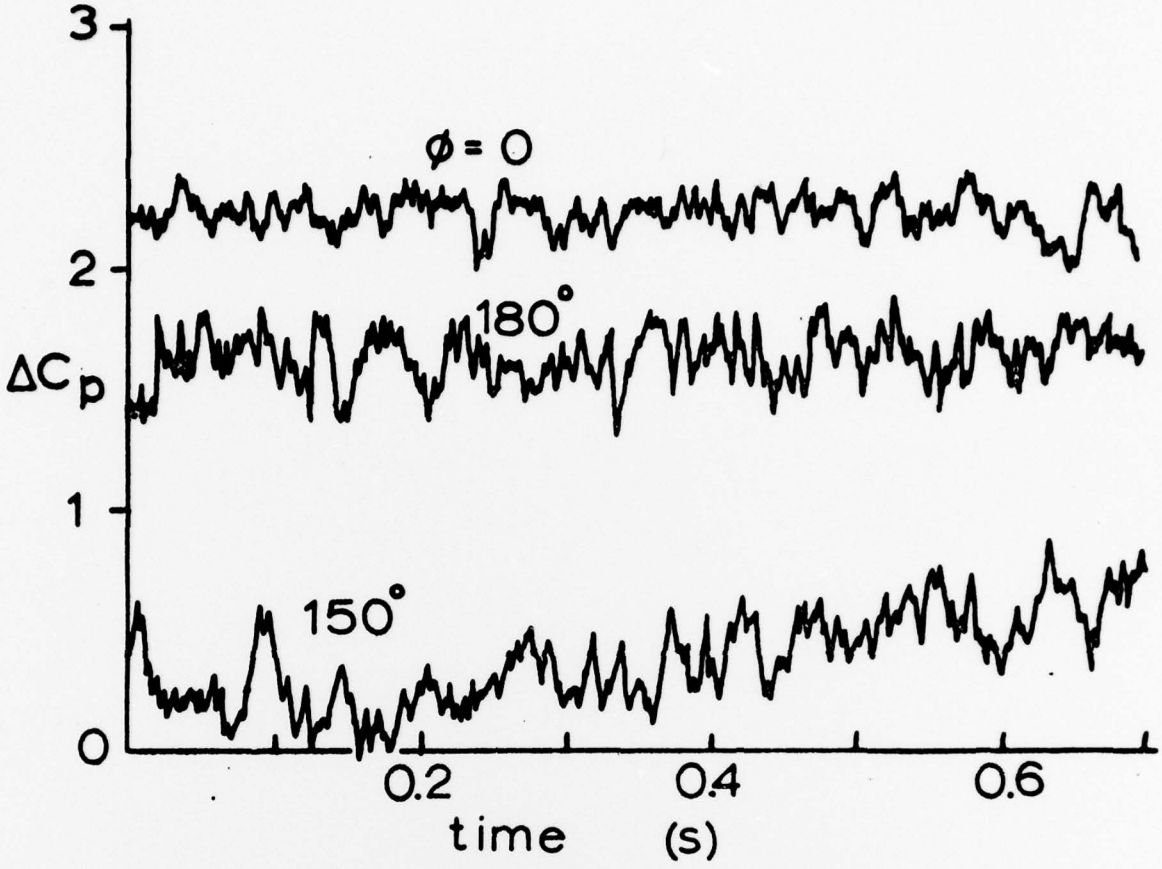

Fig. 24 The effect of roll angle on transient pressure differences for $\alpha = 50^{\circ}$, $Re = 1.0 \times 10^{5}$, $x/d = 4$

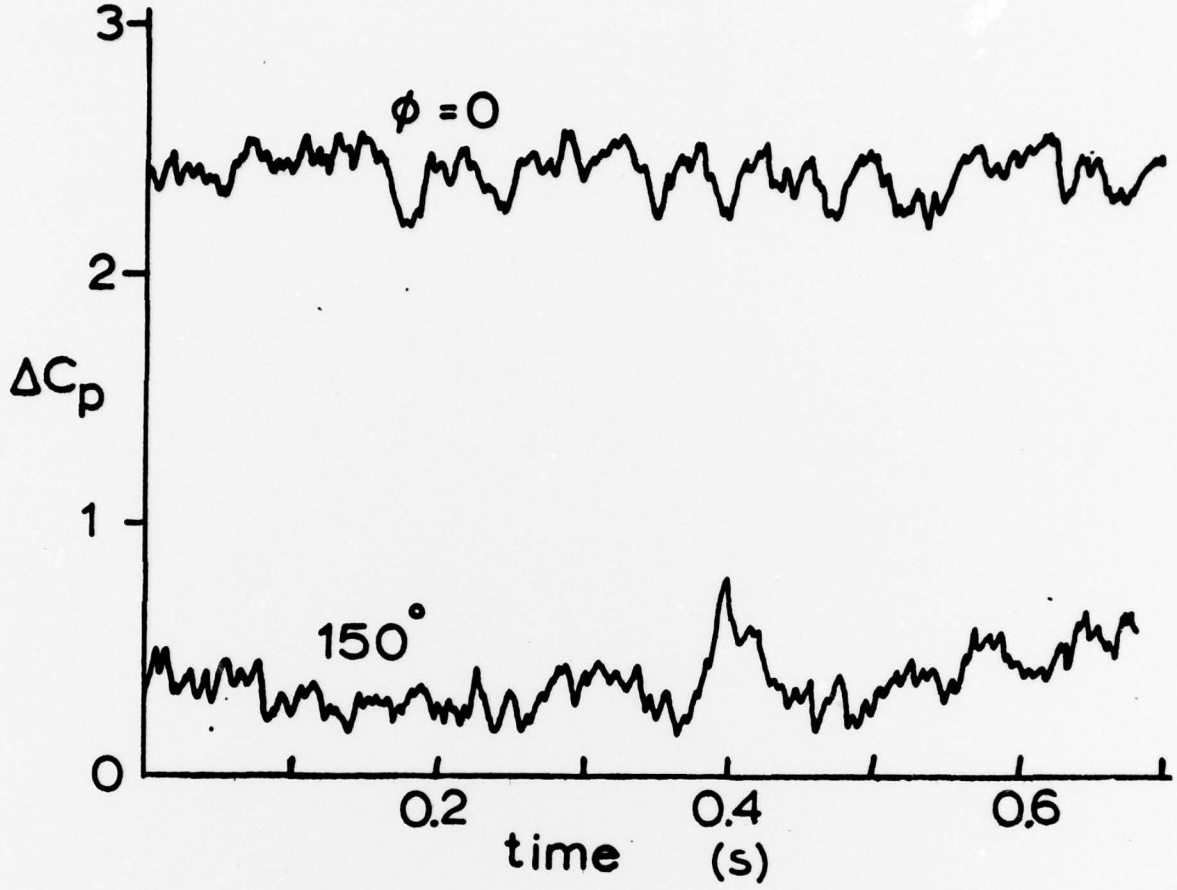

Fig. 25 The effect of roll angle on transient pressure differences for $\alpha = 50^{\circ}$, Re = 0.5 x 10^5, x/d = 4

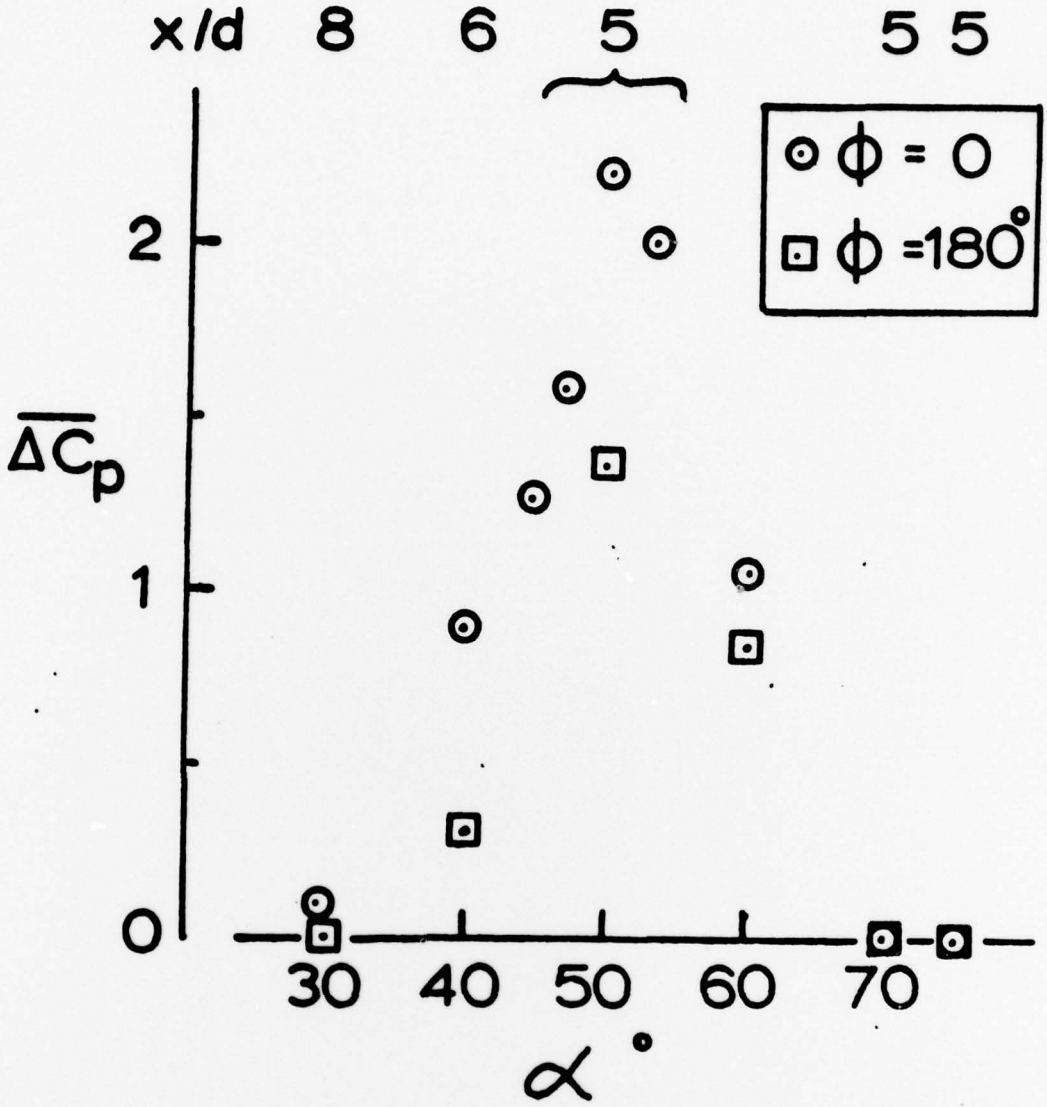

Fig. 26 Variation of mean pressure difference with angle of incidence for two roll angles at Re = 1.0×10^5, x/d = 4

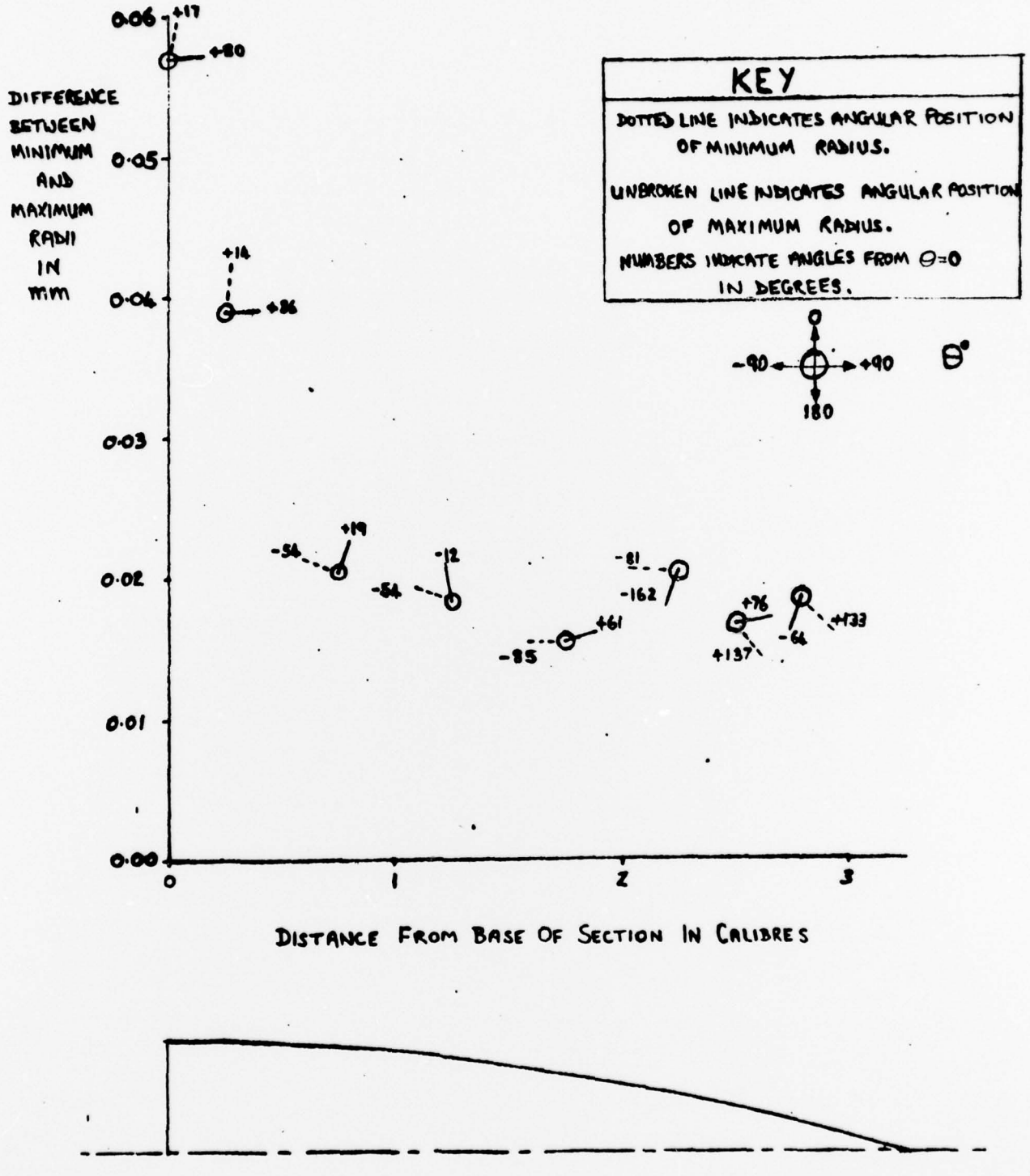

Fig. 27 Eccentricity of 3.0 calibre ogive nose

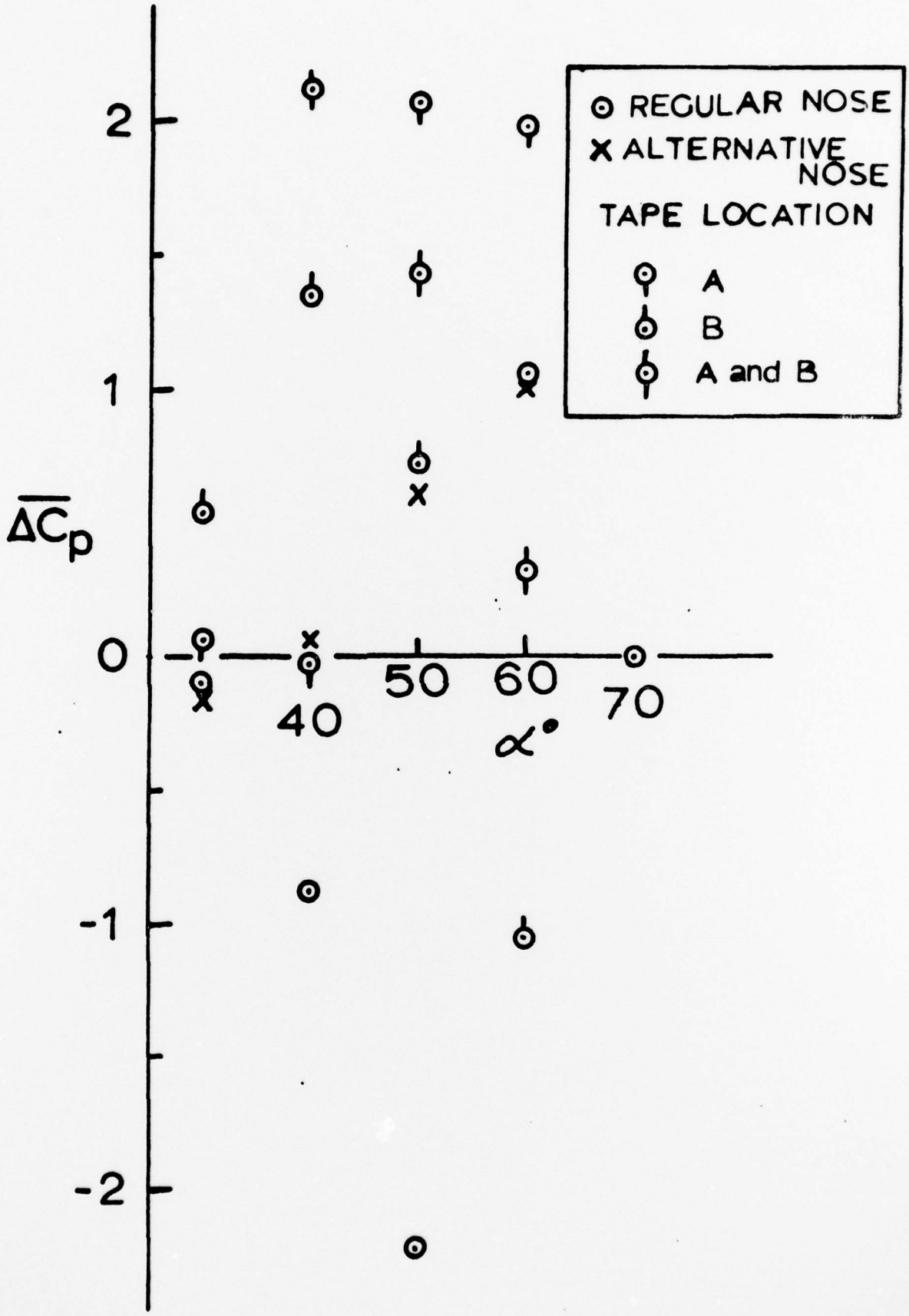

Fig. 28 Effect on mean pressure difference of minor alterations to the nose at Re = 1.0×10^5, $\phi = 0^\circ$

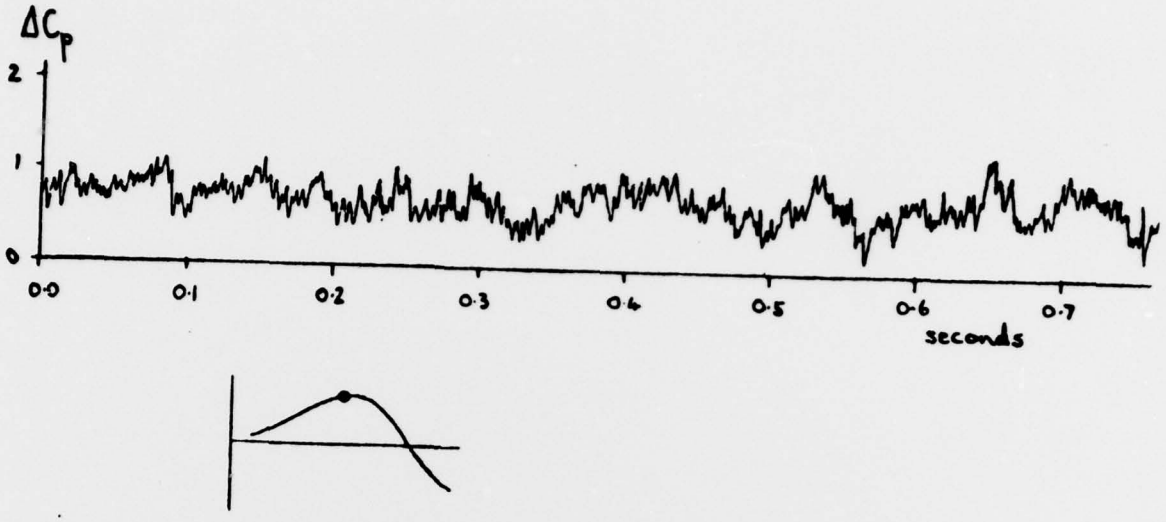

Fig. 29 Transient pressure difference for 1.0 calibre ogive nose, $\alpha = 50^{o}$, $x/d = 5$, $Re = 1.0 \times 10^{5}$

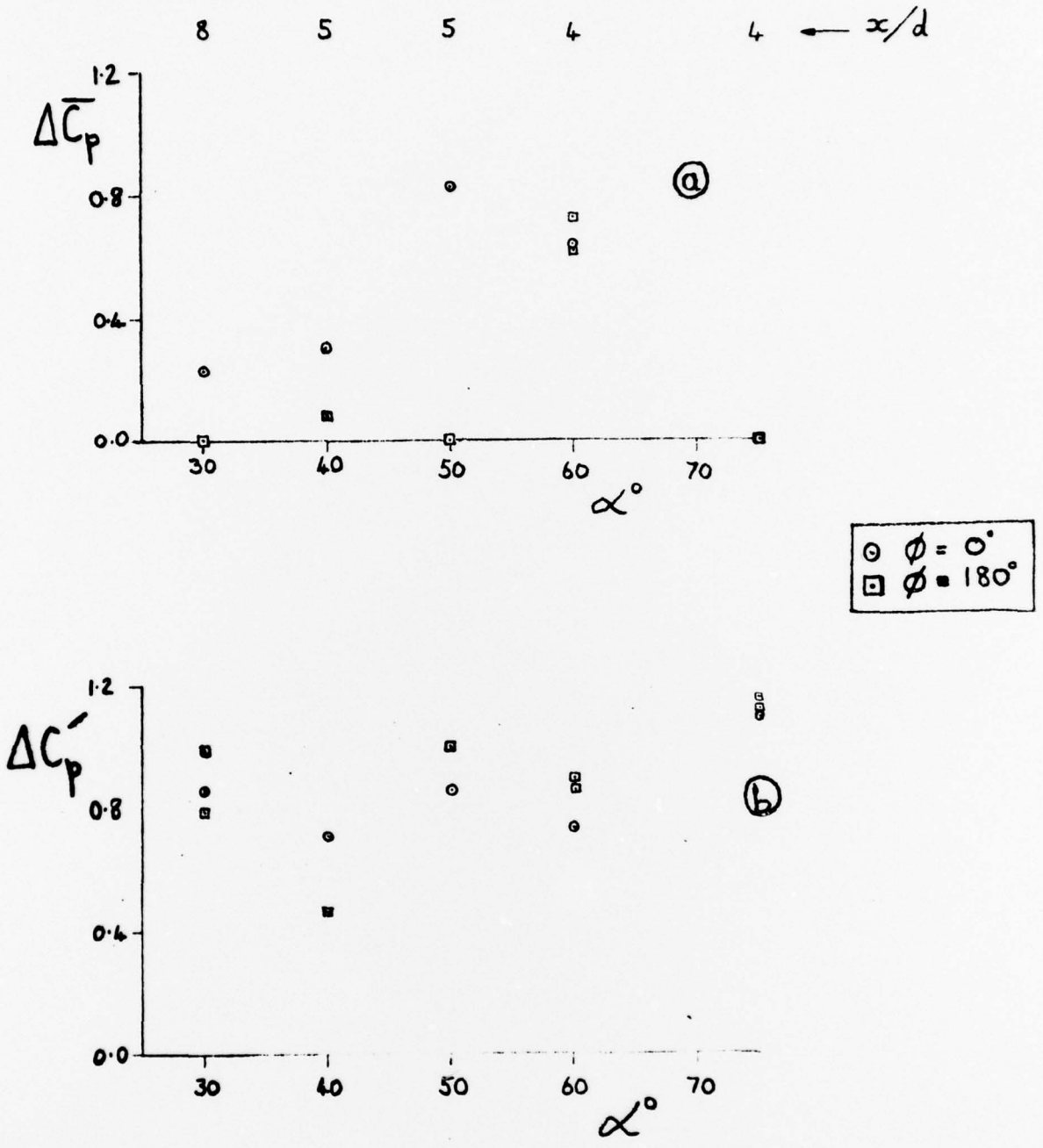

Fig. 30 Variation with incidence for 1.0 calibre ogive nose, Re = 1.0 x 10^5 of (a) mean level and (b) amplitude of fluctuating pressure differences

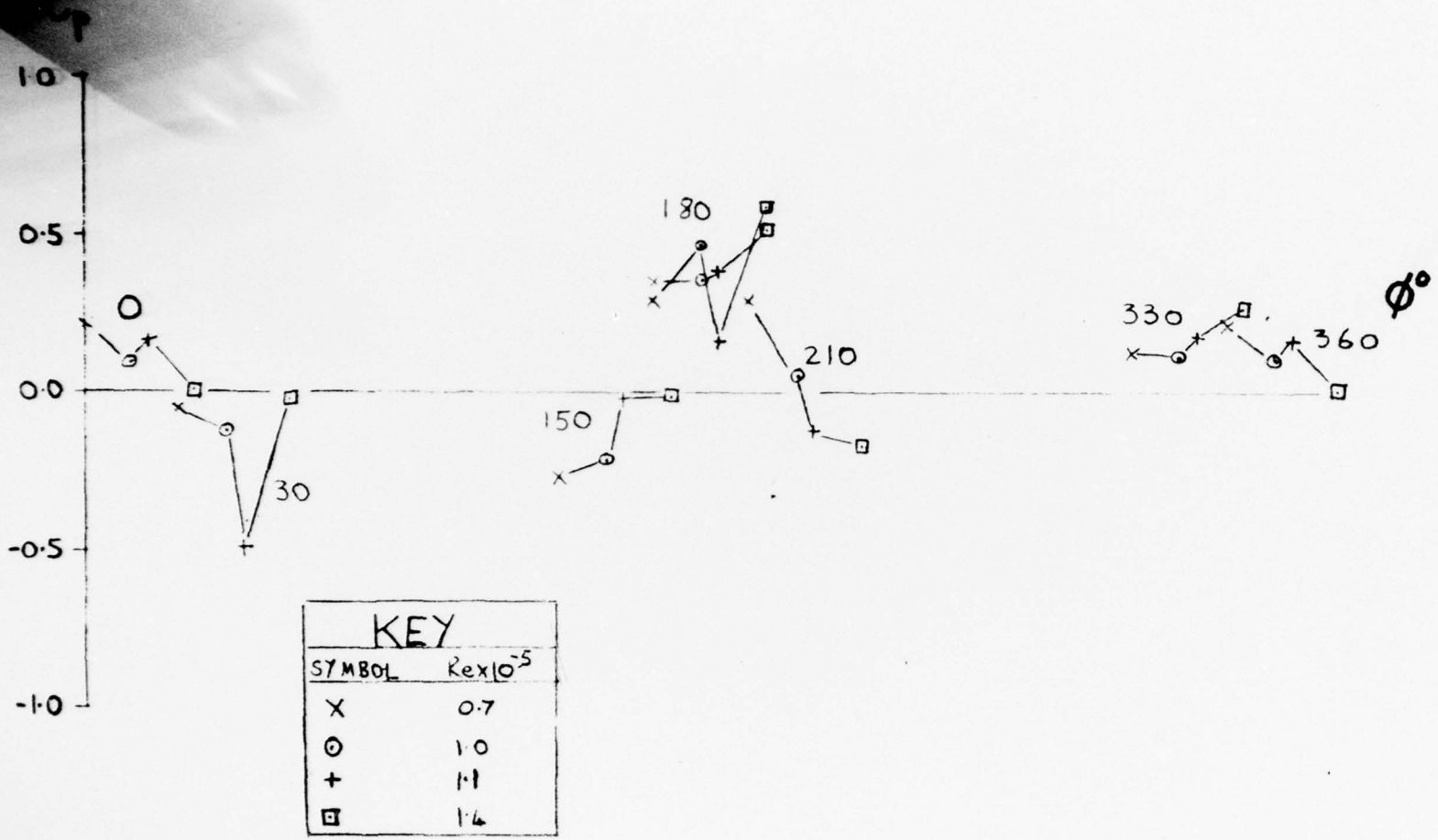

Fig. 31 The effect of roll angle and Reynolds number on mean pressure difference for 2.0 calibre ogive nose, $\alpha = 50^{\circ}$, x/d = 5

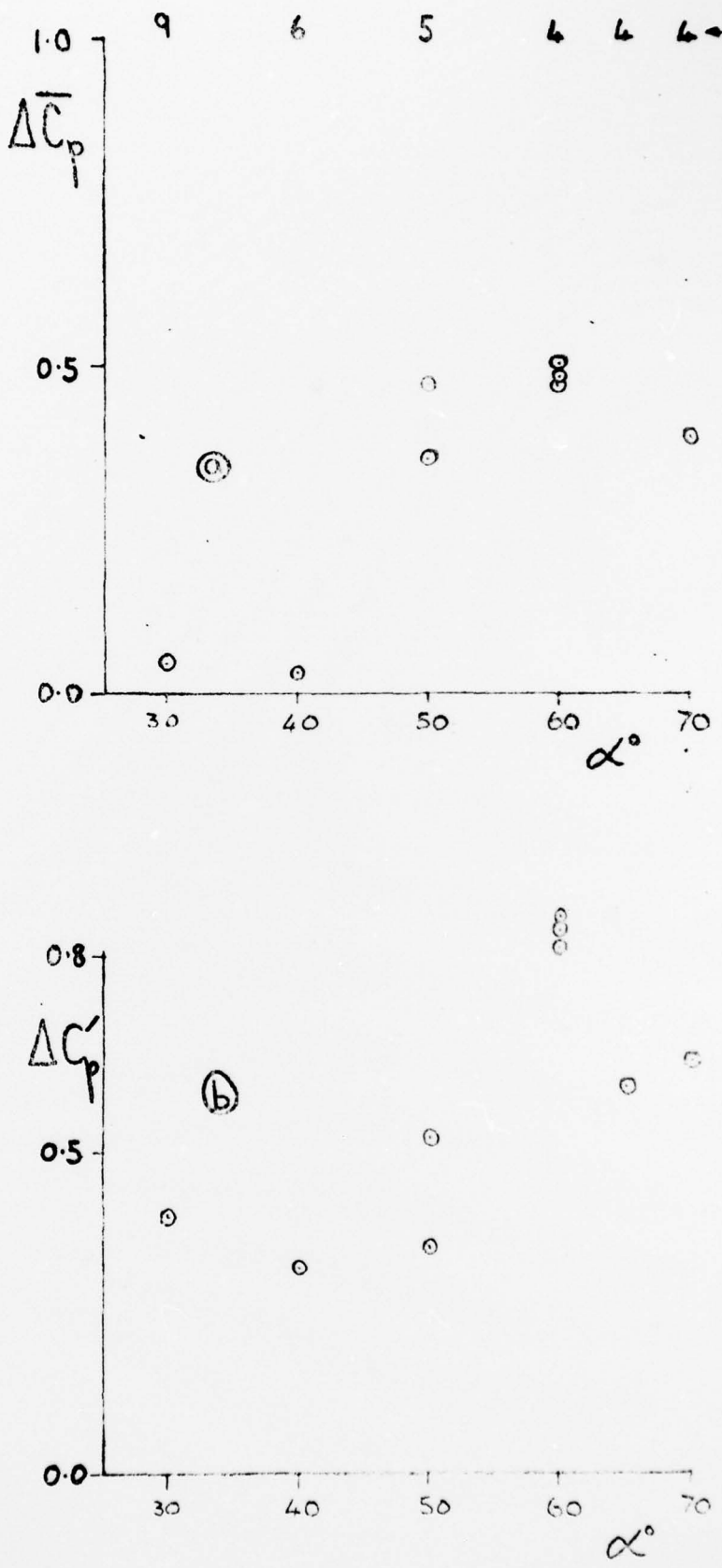

Fig. 32 Variation with incidence for 2.0 calibre ogive nose, Re = 1.0 x 10^5, $\phi = 180^\circ$ of (a) mean level and (b) amplitude of fluctuating pressure difference

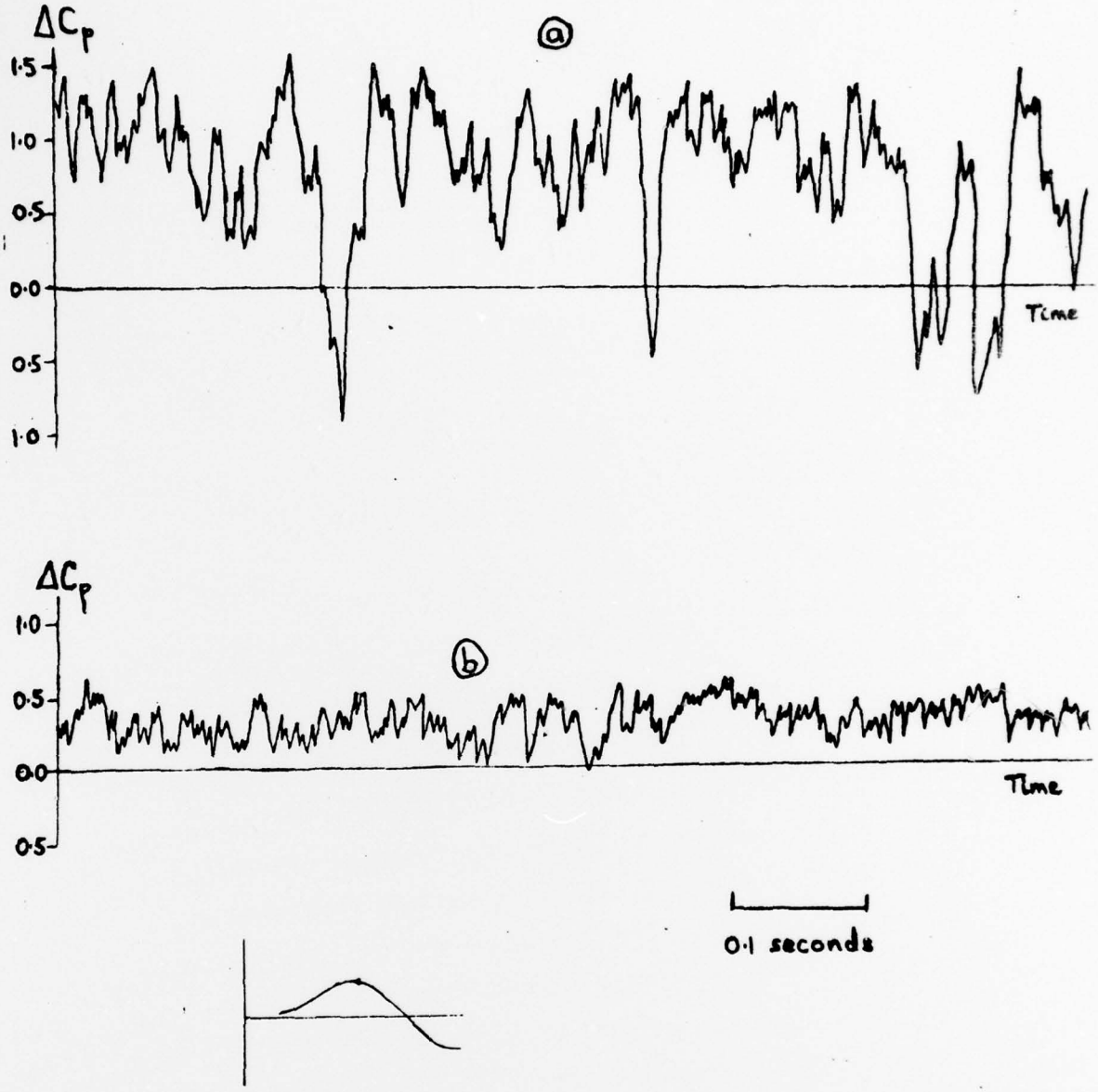

Fig. 33 Transient pressure differences for 2.0 calibre ogive nose, $\alpha = 50^{\circ}$, $Re = 1.1 \times 10^{5}$, $x/d = 5$, $\phi = 180^{\circ}$; (a) Bristol Tunnel; (b) R.A.E. tunnel

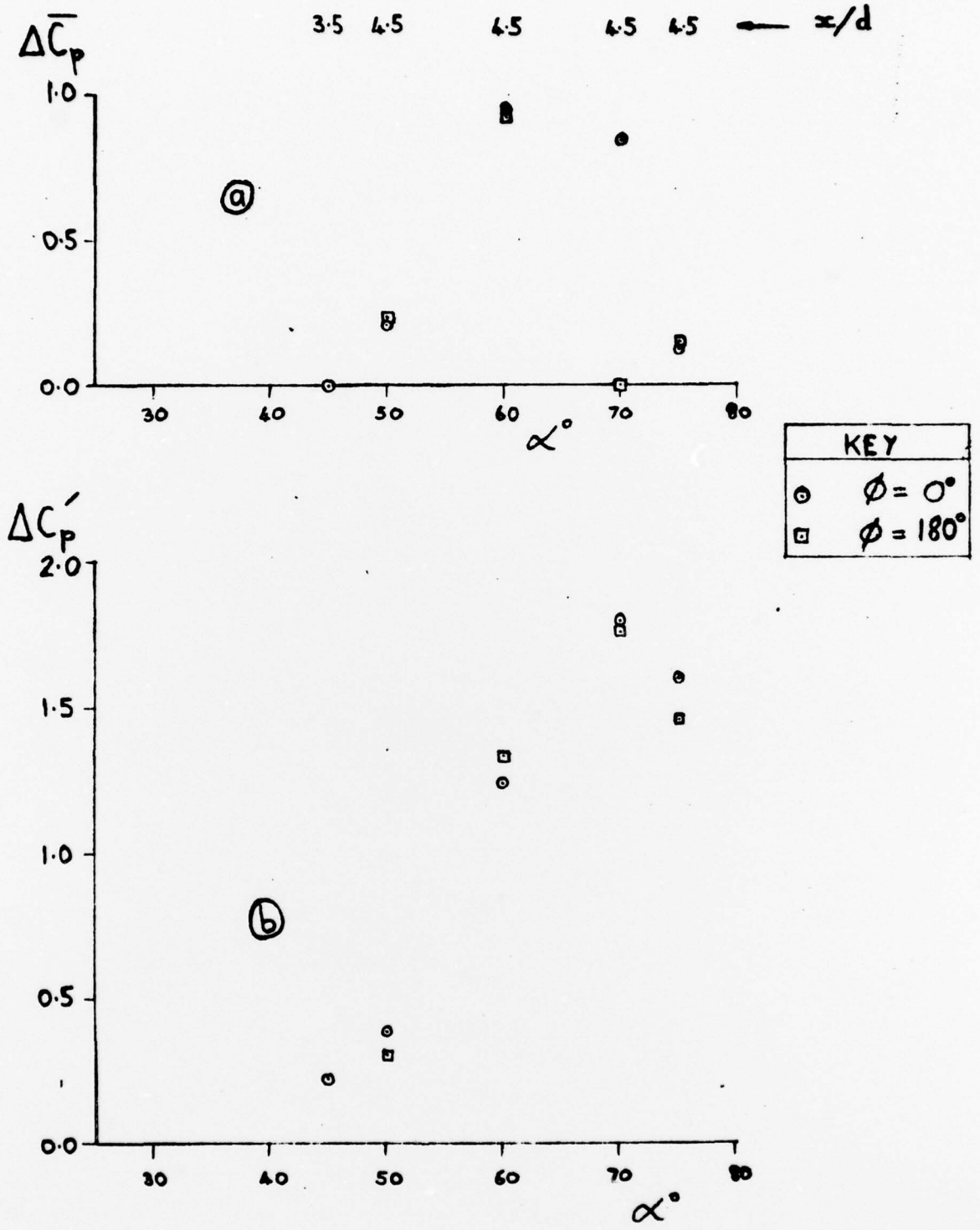

Fig. 34 Variation with incidence for 2.5 calibre ogive nose, Re = 1.0 x 10^5 of (a) mean level and (b) amplitude of fluctuating pressure difference

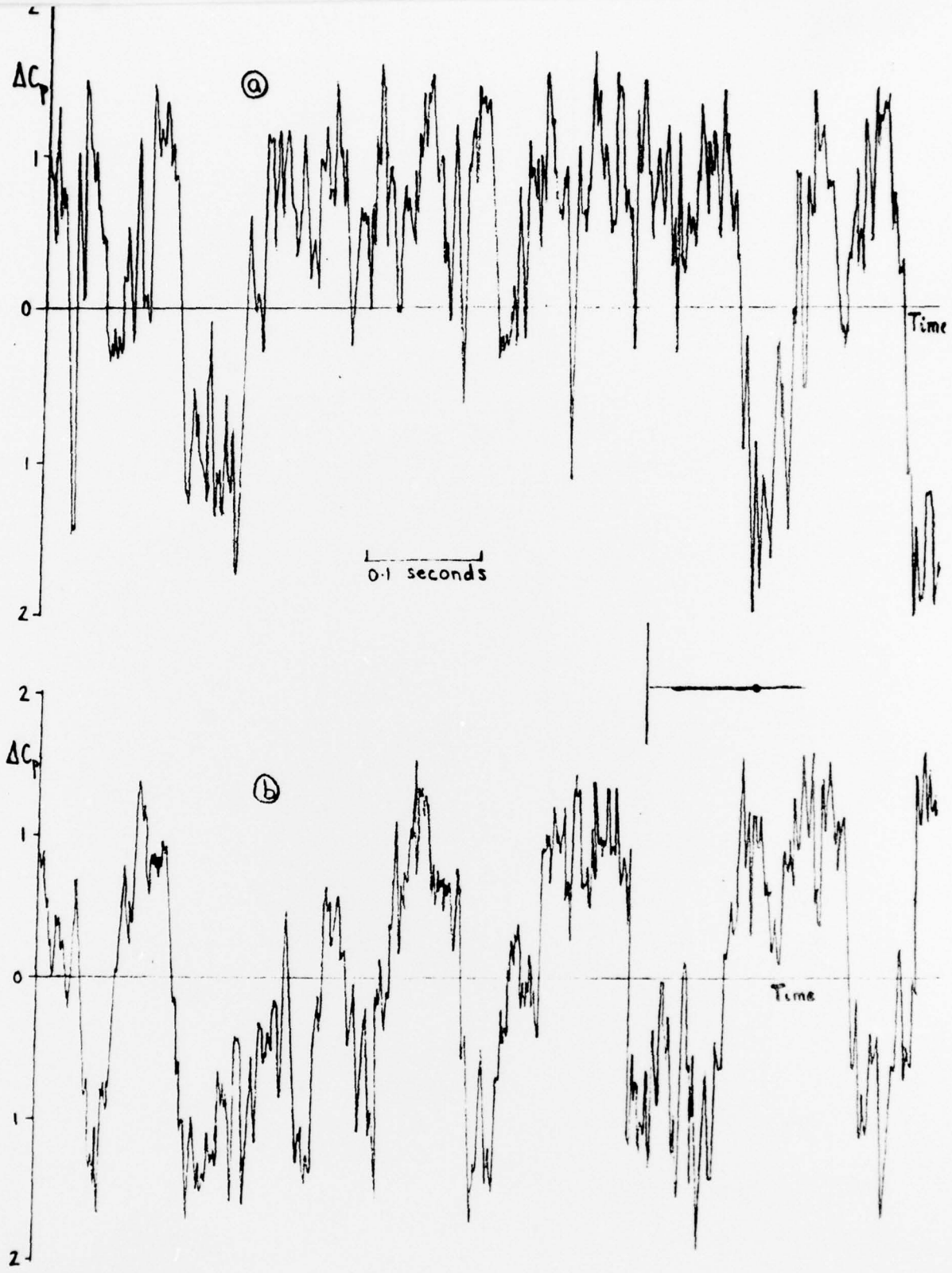

Fig. 35 Transient pressure differences for 2.5 calibre ogive nose, $\alpha = 70^{\circ}$, $x/d = 4.5$, $Re = 1.0 \times 10^{5}$; (a) $\phi = 0^{\circ}$; (b) $\phi = 180^{\circ}$

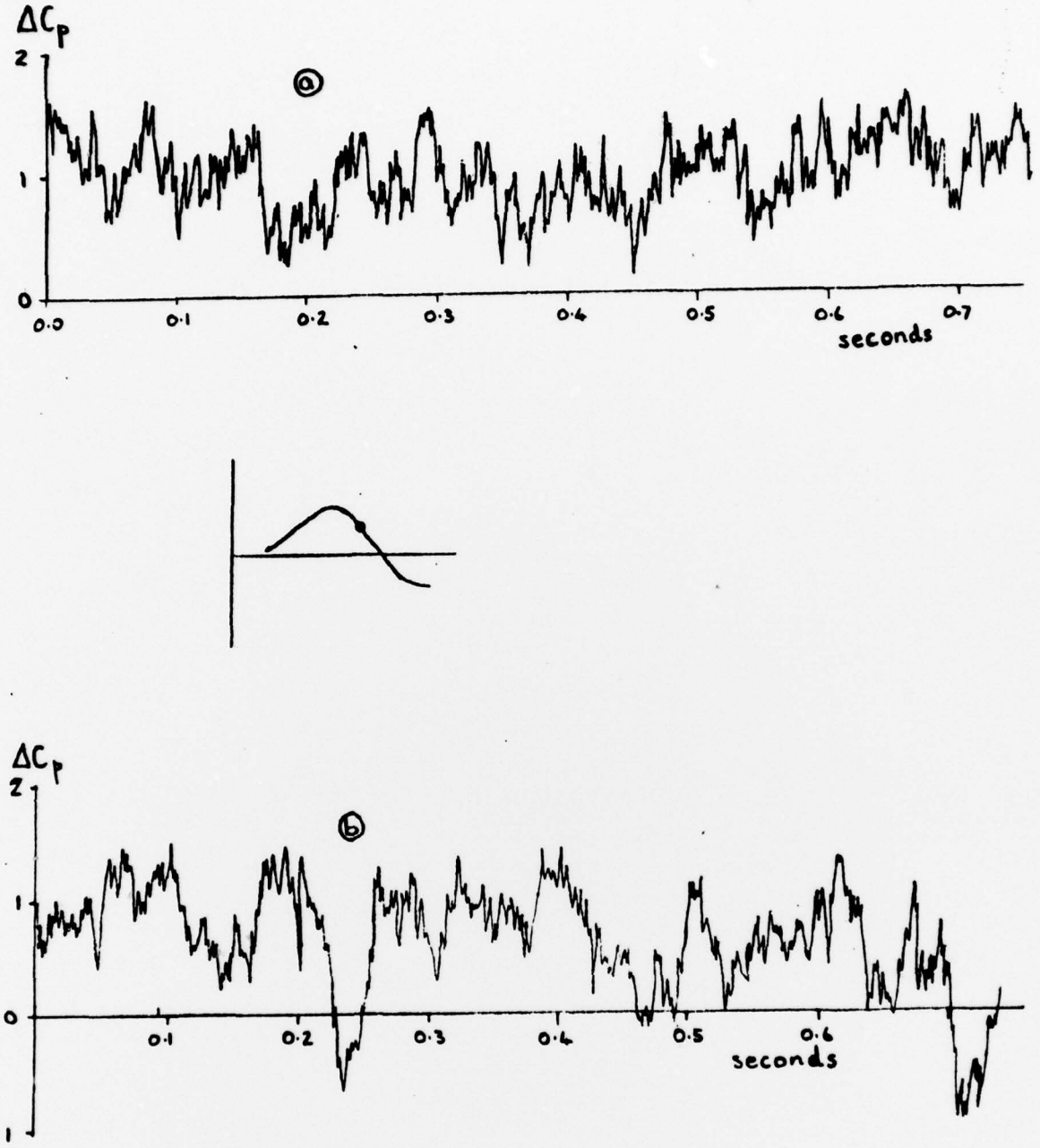

Fig. 36 Transient pressure differences for 2.5 calibre ogive nose, $\alpha = 60^{o}$, $x/d = 4.5$, $Re = 1.0 \times 10^{5}$; (a) $\phi = 0^{o}$; (b) $\phi = 180^{o}$